Modeling optical properties of liquid-crystal devices by numerical solution of time-harmonic Maxwell equations

Nandana D. Amarasinghe

Remote Sensing Systems, Santa Rosa, CA 95401

nandana@remss.com

Eugene C. Gartland, Jr.

Department of Mathematical Sciences,

Kent State University, Kent, OH 44242

gartland@math.kent.edu
http://www.math.kent.edu/∼gartland

Jack R. Kelly

CoAdna Photonics, San Jose, CA 95119

JackK@CoAdna.com

Liquid Crystal Institute,

Kent State University, Kent, OH 44242

jkelly@lci.kent.edu

We consider numerical modeling of the optical properties of devices typical of beam-steering devices based upon liquid-crystal materials: two dimensional, anisotropic and inhomogeneous dielectric properties, periodic in one dimension. A mathematical formulation of the system of second-order partial differential equations for the components of the time-harmonic electric field is discretized using a finite-element method based upon curl-conforming edge elements. The discrete equations are also interpreted as equivalent finite-difference equations. It is shown how the resulting large sparse complex system of linear algebraic equations can be solved by an iterative method with convergence accelerated by a preconditioner based upon fast Fourier transforms. Benchmarking results and the application to a realistic problem are reported. The practical limitations of the approach and its advantages and disadvantages compared to other approaches are discussed.

OCIS codes: 050.1970, 160.3710, 230.3720, 260.1180, 260.2110

1. INTRODUCTION

We are interested in the development of numerical modeling tools to assist in the design and characterization of devices based upon liquid-crystal materials, including display devices and, in particular, beam-steering devices. Features of typical devices include rectangular geometries, stratified components with planar interfaces, and a

liquid-crystal film layer with anisotropic and inhomogeneous dielectric properties. The other components that make up the device (substrates, transparent conducting layers, polarizers, retardation layers, and the like) will vary from device to device; however, in general they can be modeled either analytically or by computations that are much simpler than those required to characterize behavior of the electromagnetic fields in the film layer. While we have in mind the particular case of devices based on liquid-crystal materials, our basic ideas and approach apply to any medium that may have anisotropic and inhomogeneous optical properties.

Liquid-crystal devices have existed for a long time, and several methods have been developed to model their optical properties both mathematically and numerically. Most of these approaches have been based upon approximations that treat all of the features and properties in transverse directions as uniform, which results in mathematical models in terms of ordinary differential equations and systems. This includes, for example, all of the "matrix methods" for optics (2×2, 4×4, Jones calculus, etc.). Modern applications require numerical modeling in two and three spatial dimensions. This is driven primarily by smaller feature sizes (and the influence of fringe fields, for example) and by new devices that are based upon intrinsic two-dimensional or three-dimensional structures.

There are several different approaches to modeling the optics of such devices. Approximate techniques include quasi-one-dimensional methods (averaging in the transverse directions one-dimensional calculations), Beam Propagation Methods,[1–3] and methods based upon the Geometric Optics Approximation.[4–7] Exact methods require the solution of the Maxwell equations in some formulation. Until now this

has been accomplished using the "Finite Difference Time Domain" approach.[8–13] In this paper, we discuss a method for solving a formulation in the frequency domain, i.e., for the time-harmonic form of the Maxwell equations. Such techniques have been used by numerical analysts in other settings.[14] Our objectives have been to develop effective ways to apply these techniques to our particular problems and to explore their limitations and their advantages and disadvantages compared to other approaches and approximations in this context.

The literature concerned with optics and electromagnetics in general (analytical and computational aspects) is vast and is distributed among physics, engineering, and mathematics, with different notations and terminologies sometimes used. We have relied upon certain standard or representative references in each area: Born and Wolff,[15] Jackson[16] (physics); Peterson, Ray, and Mittra[17] (engineering); and Cessenat,[18] Nédélec[19] (mathematics).

2. PROBLEM AND FORMULATION

As a prototype of a liquid-crystal beam-steering device, we consider the generic model system depicted in Fig. 1. We assume that the device is of infinite extent in the x and z directions with all properties $2L$ periodic in x and uniform in z. Figure 1 displays the x-y section of one periodic cell. The dielectric properties of the film layer Ω (which is of thickness d in the y direction) can be anisotropic as well as spatially varying. The front and back components (which meet the liquid-crystal layer at interfaces Γ_1 and Γ_2) will differ from device to device and will consist of typical elements such as confining substrates, polarizers, retardation layers, and the like. We assume that they also are

$2L$ periodic in x and uniform in z and that their separate optical properties can be modeled either by analytical formulas or by auxiliary numerical computations. The exact composition of the front and back components does not matter in the approach we take.

We assume that the properties of the materials and the intensity of the radiation are in the linear regime, with a scalar magnetic-permeability tensor that differs by a negligible amount from vacuum and a dielectric tensor that may be complex and not necessarily Hermitian:

$$\boldsymbol{\mu} = \mu_0 \boldsymbol{I}, \quad \boldsymbol{\epsilon}(\mathbf{r}) = \epsilon_0 \boldsymbol{\epsilon}_{\mathrm{r}}(x, y), \tag{1}$$

where $\boldsymbol{I}$ is the identity tensor and the relative dielectric tensor satisfies the periodicity assumptions

$$\boldsymbol{\epsilon}_{\mathrm{r}}(x + 2L, y) = \boldsymbol{\epsilon}_{\mathrm{r}}(x, y), \qquad -\infty < x < \infty, \quad 0 < y < d. \tag{2}$$

Thus we allow for media that are absorbing or not; however, we do not admit chiral or optically active materials in the present development. The device is illuminated from below by a monochromatic plane-wave source of arbitrary polarization incident from an arbitrary direction in the x-y plane. Our objective is to determine the composition of the reflected and transmitted light.

We use a mathematical formulation for the total electric and magnetic fields $\mathrm{Re}[\exp(-i\omega t)\mathbf{E}(\mathbf{r})]$ and $\mathrm{Re}[\exp(-i\omega t)\mathbf{H}(\mathbf{r})]$, in which the complex spatial parts or

"amplitudes" satisfy (in the absence of current densities)

$$\nabla \times \mathbf{E} = i\omega\mu_0\mathbf{H}, \tag{3}$$

$$\nabla \times \mathbf{H} = -i\omega\boldsymbol{\epsilon}\mathbf{E}. \tag{4}$$

By virtue of the relation $\nabla \cdot (\nabla \times \mathbf{v}) = 0$ (valid for any sufficiently smooth vector field $\mathbf{v}$), solutions of these equations necessarily satisfy the remaining Maxwell equations (in the absence of charge densities)

$$\nabla \cdot \mathbf{D} = \nabla \cdot \mathbf{B} = 0, \tag{5}$$

with the constitutive relations

$$\mathbf{D} = \boldsymbol{\epsilon}\mathbf{E}, \quad \mathbf{B} = \mu_0\mathbf{H}. \tag{6}$$

A well-posed problem can be formulated for the total $\mathbf{E}$ field alone by eliminating $\mathbf{H}$, which gives

$$\nabla \times (\nabla \times \mathbf{E}) - k^2\boldsymbol{\epsilon}_{\mathrm{r}}(x, y)\mathbf{E} = \mathbf{0}. \tag{7}$$

Here we allow for a complex wavenumber of the form

$$k = k_0(1 + i\kappa), \quad k_0 = \omega\sqrt{\mu_0\epsilon_0}, \tag{8}$$

where $\kappa \geq 0$ is a real nonnegative "attenuation coefficient," which we introduce primarily for numerical purposes to eliminate resonances, as has been done by others.[20] The non-absorbing solution is obtained in general in the limit as $\kappa \to 0$ according to the "Limiting Absorption Principle.[18]" These solutions give the spatial parts of the steady state solutions for the corresponding time-dependent Maxwell equations according to the "Limiting Amplitude Principle.[18]"

The incident field is assumed to be of the form

$$\mathbf{E}_{\mathrm{inc}}(\mathbf{r}) = \exp(i\mathbf{k}\cdot\mathbf{r})\mathbf{E}_0^{\mathrm{inc}}, \tag{9}$$

where $\mathbf{k} = (k_x, k_y, 0) = k\hat{\mathbf{u}}$, with $\hat{\mathbf{u}}$ a real propagation direction (unit vector) in x-y. Here we must also have

$$\mathbf{k}\cdot\mathbf{k} = k^2, \quad \mathbf{k}\cdot\mathbf{E}_0^{\mathrm{inc}} = 0. \tag{10}$$

The solution fields are "quasi-periodic," $\mathbf{E}(x+2L, y) = \exp(i2k_xL)\mathbf{E}(x, y)$, and satisfy the "Floquet-Bloch conditions":

$$\mathbf{E}_{\mathrm{T}}(L, y) = \exp(i2k_xL)\mathbf{E}_{\mathrm{T}}(-L, y), \tag{11}$$

$$(\nabla\times\mathbf{E})_{\mathrm{T}}(L, y) = \exp(i2k_xL)(\nabla\times\mathbf{E})_{\mathrm{T}}(-L, y). \tag{12}$$

Here $\mathbf{E}_{\mathrm{T}}$ denotes the *tangential* components of $\mathbf{E}$: (E_y, E_z) along $x = \text{const}$ (as above), (E_x, E_z) on the front and back interfaces Γ_1 and Γ_2 (see Fig. 1) or along any $y = \text{const}$.

The electromagnetic fields satisfy the usual interface conditions: continuity of the tangential components of $\mathbf{E}$ and $\mathbf{H}$ and the normal components of $\mathbf{D}$ and $\mathbf{B}$ across any material interface with discontinuous dielectric properties. Thus $\mathbf{E}_{\mathrm{T}}$ and $(\nabla\times\mathbf{E})_{\mathrm{T}}$ (by virtue of Eq. (3) and the constancy of μ_0) are continuous everywhere. The following radiation conditions are satisfied: $\mathbf{E} - \mathbf{E}_{\mathrm{inc}}$ is outward propagating as $y \to -\infty$, as is the total field $\mathbf{E}$ as $y \to \infty$. For prescribed k_0, d, L, $\boldsymbol{\epsilon}_{\mathrm{r}}$, and $\mathbf{E}_{\mathrm{inc}}$, the second-order vector partial differential equation (7), the Floquet-Bloch conditions (11) and (12), the interface conditions, and the radiation conditions are expected to give a well-posed mathematical problem for the time-harmonic electric field $\mathbf{E}$ for any $\kappa > 0$ or with $\kappa = 0$ for all but possibly a finite set of incidence directions, as is the case in other similar settings.[21–23]

3. FINITE FORMULATION

Our problem thus far is posed on an infinite domain: $-L < x < L$ (plus quasi-periodic conditions at $x = \pm L$), $-\infty < y < \infty$ (plus radiation conditions as $y \to \pm\infty$). It must somehow be reduced to a *finite* computational domain. We do this now by modeling analytically the parts of the problem domain exterior to the liquid-crystal film layer (that is, $y < 0$ and $y > d$). For this and for subsequent numerical discretization, it is more convenient to work with a "weak formulation" of the problem, which we describe now.

A. Weak Formulation

Integrating Eq. (7) against a sufficiently smooth test field $\mathbf{F}(x, y)$ and performing an integration by parts gives

$$\int_\Omega \{(\nabla \times \mathbf{E}) \cdot (\nabla \times \mathbf{F}^*) - k^2[\boldsymbol{\epsilon}_\mathrm{r}(x, y)\mathbf{E}] \cdot \mathbf{F}^*\} + \int_{\partial\Omega} [\hat{\boldsymbol{\nu}} \times (\nabla \times \mathbf{E})] \cdot \mathbf{F}^* = 0. \qquad (13)$$

Here $\partial\Omega$ denotes the boundary of Ω (the front and back interfaces Γ_1 and Γ_2, plus the edges along $x = \pm L$), $\hat{\boldsymbol{\nu}}$ is the outward unit normal vector on the boundary, and $\mathbf{F}^*$ denotes the component-wise complex conjugate of $\mathbf{F}$. Thus the boundary integrals involve only the tangential components of $\nabla \times \mathbf{E}$ and $\mathbf{F}$. If $\mathbf{E}$ satisfies Eq. (12) and $\mathbf{F}$ satisfies the complementary Floquet-Bloch condition (with k_x replaced by its complex conjugate k_x^*)

$$\mathbf{F}_\mathrm{T}(L, y) = \exp(i2k_x^* L)\mathbf{F}_\mathrm{T}(-L, y), \qquad (14)$$

then the integrals along the left-side and right-side boundary edges ($x = -L$ and $x = L$) cancel, leaving the following equation, which must be satisfied by any quasi-

periodic solution of Eq. (7) and for all test fields $\mathbf{F}$ satisfying Eq. (14):

$$\int_{\Omega}\{(\nabla\times\mathbf{E})\cdot(\nabla\times\mathbf{F}^*)-k^2[\boldsymbol{\epsilon}_{\mathrm{r}}(x,y)\mathbf{E}]\cdot\mathbf{F}^*\}+\int_{\Gamma_1+\Gamma_2}[\hat{\boldsymbol{\nu}}\times(\nabla\times\mathbf{E})]_{\mathrm{T}}\cdot\mathbf{F}^*_{\mathrm{T}}=0. \quad (15)$$

We note that the coupling between the interior and exterior solutions is through $(\nabla\times\mathbf{E})_{\mathrm{T}}$ on Γ_1 and Γ_2.

B. Admittance Maps

The solution outside Ω satisfies the relevant strong or weak formulation of the Maxwell equations and couples to the interior solution via the continuity of $\mathbf{E}_{\mathrm{T}}$ and $(\nabla\times\mathbf{E})_{\mathrm{T}}$ across Γ_1 and Γ_2. The structure of the front and back components will vary from device to device. We assume that they can be characterized analytically or via auxiliary calculations. Thus we assume that given prescribed values of the tangential components of the total field on the interfaces, $\mathbf{E}_{\mathrm{T}}(\cdot,0)$ and $\mathbf{E}_{\mathrm{T}}(\cdot,d)$, we can determine the outer fields that correspond to those boundary values and satisfy the relevant equations and auxiliary conditions and which are outward radiating as $y\to\pm\infty$. In terms of these outer solutions, which we denote $\mathbf{E}_1(x,y)$ in $y<0$ and $\mathbf{E}_2(x,y)$ in $y>d$, we define "admittance maps" (also known as "Calderon operators" or "Poincaré-Steklov operators")[18,19] $\mathbf{C}_1$ and $\mathbf{C}_2$ via

$$\mathbf{C}_1:\mathbf{E}_{\mathrm{T}}(\cdot,0)\mapsto[-\hat{\mathbf{y}}\times(\nabla\times\mathbf{E}_1)]_{\mathrm{T}}(\cdot,0-), \quad (16)$$

$$\mathbf{C}_2:\mathbf{E}_{\mathrm{T}}(\cdot,d)\mapsto[+\hat{\mathbf{y}}\times(\nabla\times\mathbf{E}_2)]_{\mathrm{T}}(\cdot,d+). \quad (17)$$

The exterior problems for $\mathbf{E}_1$ and $\mathbf{E}_2$ will be well posed in general and typically can be constructed in terms of superpositions of plane waves, which we do in the next section for the simple example of a single glass substrate. In the absence of any

external illumination (i.e., $\mathbf{E}_{\rm inc} = \mathbf{0}$, for which the solution to the full problem would be the *zero* field everywhere), we then would have

$$\int_\Omega \{(\nabla\times\mathbf{E})\cdot(\nabla\times\mathbf{F}^*) - k^2[\boldsymbol{\epsilon}_{\rm r}(x,y)\mathbf{E}]\cdot\mathbf{F}^*\} + \int_{\Gamma_1} \mathbf{C}_1(\mathbf{E}_{\rm T})\cdot\mathbf{F}^*_{\rm T} + \int_{\Gamma_2} \mathbf{C}_2(\mathbf{E}_{\rm T})\cdot\mathbf{F}^*_{\rm T} = 0. \quad (18)$$

In this formulation, then, the exterior regions are effectively replaced by *non-local* boundary conditions on Γ_1 and Γ_2, as the values of $\mathbf{C}(\mathbf{E}_{\rm T})$ depend on $\mathbf{E}_{\rm T}$ on the *entire* interface. Such boundary conditions are referred to as "exact radiation boundary conditions[17]" or "transparent boundary conditions[14]" and are closely related to "Dirichlet to Neumann maps" and techniques for exterior problems discussed in Ref. 24.

C. Equivalent Surface Current

The only source driving our solution is the incident field $\mathbf{E}_{\rm inc}$ radiating inward from below. The total field in the exterior front can be decomposed $\mathbf{E} = \mathbf{E}_1 + \mathbf{E}_3$, where $\mathbf{E}_1$ is the exterior solution associated with the admittance map $\mathbf{C}_1$ above (which satisfies $\mathbf{E}_{1\rm T} = \mathbf{E}_{\rm T}$ on Γ_1 and radiates outward as $y \to -\infty$) and where $\mathbf{E}_3$ satisfies $\mathbf{E}_{3\rm T} = \mathbf{0}$ on Γ_1 and is such that $\mathbf{E}_3 - \mathbf{E}_{\rm inc}$ is outward radiating as $y \to -\infty$. Note that the boundary condition on $\mathbf{E}_3$ is that of a perfect electrical conductor.

The $\mathbf{E}_3$ solution embodies the influence of $\mathbf{E}_{\rm inc}$ and can be used to drive the total field in the interior through an "equivalent surface current" on the interface Γ_1:

$$\begin{aligned}\int_\Omega &\{(\nabla\times\mathbf{E})\cdot(\nabla\times\mathbf{F}^*) - k^2[\boldsymbol{\epsilon}_{\rm r}(x,y)\mathbf{E}]\cdot\mathbf{F}^*\} \\ &+ \int_{\Gamma_1} \mathbf{C}_1(\mathbf{E}_{\rm T})\cdot\mathbf{F}^*_{\rm T} + \int_{\Gamma_1} [\hat{\boldsymbol{\nu}}\times(\nabla\times\mathbf{E}_3)]_{\rm T}\cdot\mathbf{F}^*_{\rm T} + \int_{\Gamma_2} \mathbf{C}_2(\mathbf{E}_{\rm T})\cdot\mathbf{F}^*_{\rm T} = 0, \quad (19)\end{aligned}$$

or

$$\int_\Omega \{(\nabla \times \mathbf{E}) \cdot (\nabla \times \mathbf{F}^*) - k^2[\boldsymbol{\epsilon}_{\mathrm{r}}(x,y)\mathbf{E}] \cdot \mathbf{F}^*\} + \int_{\Gamma_1} \mathbf{C}_1(\mathbf{E}_{\mathrm{T}}) \cdot \mathbf{F}^*_{\mathrm{T}} + \int_{\Gamma_2} \mathbf{C}_2(\mathbf{E}_{\mathrm{T}}) \cdot \mathbf{F}^*_{\mathrm{T}} = \int_{\Gamma_1} \mathbf{g}_{1\mathrm{T}}(x) \cdot \mathbf{F}^*_{\mathrm{T}}, \tag{20}$$

with

$$\mathbf{g}_1(x) = \hat{\mathbf{y}} \times (\nabla \times \mathbf{E}_3)(x, 0-). \tag{21}$$

We can express Eq. (20) in the functional form

$$a(\mathbf{E}, \mathbf{F}) = l(\mathbf{F}), \tag{22}$$

with the forms $a(\cdot,\cdot)$ and $l(\cdot)$ defined by

$$a(\mathbf{E}, \mathbf{F}) = \int_\Omega \{(\nabla \times \mathbf{E}) \cdot (\nabla \times \mathbf{F}^*) - k^2[\boldsymbol{\epsilon}_{\mathrm{r}}(x,y)\mathbf{E}] \cdot \mathbf{F}^*\} + \int_{\Gamma_1} \mathbf{C}_1(\mathbf{E}_{\mathrm{T}}) \cdot \mathbf{F}^*_{\mathrm{T}} + \int_{\Gamma_2} \mathbf{C}_2(\mathbf{E}_{\mathrm{T}}) \cdot \mathbf{F}^*_{\mathrm{T}} \tag{23}$$

and

$$l(\mathbf{F}) = \int_{\Gamma_1} \mathbf{g}_{1\mathrm{T}}(x) \cdot \mathbf{F}^*_{\mathrm{T}}. \tag{24}$$

This then is our finite formulation. The nature of the front and back components has been abstracted into the admittance maps $\mathbf{C}_1$ and $\mathbf{C}_2$, and the influence of the incident radiation has been transformed into the equivalent surface current $\mathbf{g}_1$. The total field in the interior must satisfy the single Floquet-Bloch condition (11)—the second condition, Eq. (12), is a "natural" boundary condition that is satisfied automatically as a consequence of our variational formulation—and must satisfy Eq. (22) for all sufficiently smooth test fields $\mathbf{F}$ that conform to the complementary Floquet-Bloch condition, Eq. (14).

4. RAYLEIGH SERIES AND ADMITTANCE MAPS

A. Rayleigh Series Expansions

In the free spaces outside of the device, or in any homogeneous isotropic strata of the front or back components, the solution fields can be represented in terms of "Rayleigh series[18]" (also known as "plane-wave expansions," "angular spectrum representations," or "Floquet-harmonic expansions"):[17]

$$\mathbf{E}(x,y) = \sum_{n=-\infty}^{\infty} \exp[i\lambda_n x \pm i\mu_n(y-y_0)]\mathbf{E}_n, \tag{25}$$

where

$$\lambda_n = k_x + \frac{n\pi}{L}, \quad \mu_n = \sqrt{k^2 - \lambda_n^2}, \qquad n = -\infty, \ldots, \infty, \tag{26}$$

and we choose the value of the square root that is either real and non-negative or has positive imaginary part (i.e., for a complex number z in polar form, $z = \rho\exp(i\varphi),\ \rho \geq 0,\ 0 \leq \varphi < 2\pi \ \Rightarrow\ \sqrt{z} = \sqrt{\rho}\exp(i\varphi/2),\ 0 \leq \varphi/2 < \pi$)—recall that k_x and k^2 can be complex in general. The positive sign in the exponential in the sum in Eq. (25) corresponds to plane waves that radiate outwards as $y \to \infty$, while those associated with the negative sign propagate in the opposite direction.

The expansion point y_0 is arbitrary—although it must be either outside the device or in a homogeneous, isotropic stratum—and the complex amplitudes are given by

$$\mathbf{E}_n = \frac{1}{2L}\int_{-L}^{L} \exp(-i\lambda_n x)\mathbf{E}(x,y_0)\,\mathrm{d}x. \tag{27}$$

Gauss's Law in such a medium takes the form $\nabla\cdot\mathbf{E} = 0$ and implies the relation

$$\lambda_n E_{nx} \pm \mu_n E_{ny} = 0, \tag{28}$$

which can be used to determine E_{ny} from E_{nx}, provided $\mu_n \neq 0$. This will be the case whenever the attenuation coefficient is positive, $\kappa > 0$ in Eq. (8), in which case all modes are attenuated. If $\kappa = 0$, then $k = k_0 > 0$, and we will have a finite number of propagating modes (for which $-k_0 < \lambda_n < k_0$) and an infinite number of non-propagating (evanescent) modes (with either $\lambda_n < -k_0$ or $\lambda_n > k_0$). For a finite number of angles of incidence, it is possible to have one (or two) "surface modes," corresponding to $\lambda_n = \pm k_0$ and, as a consequence, $\mu_n = 0$. These cases are degenerate and admit the possibility that the full problem is not well posed (has nontrivial solutions for $\mathbf{E}_{\rm inc} = \mathbf{0}$), a so-called "resonance" phenomenon.[21–23]

B. Admittance Map for Glass Substrates

Expansions such as above can be used to construct analytical representations for the admittance maps $\mathbf{C}_1$ and $\mathbf{C}_2$ of Eqs. (16) and (17), as well as for the equivalent surface current $\mathbf{g}_1$ of Eq. (21), when the front and back components are sufficiently simple. We do so now for the case in which these consist of single glass substrates. Thus we consider a component of thickness a made up of a homogeneous, isotropic medium of index of refraction $n_{\rm r} > 1$ relative to the exterior free space.

In Appendix A, we derive an expression for the external field $\mathbf{E}_1$ associated with the Calderon operator $\mathbf{C}_1$ for this case. From it we can calculate the value of $\mathbf{C}_1$ using Eq. (16). The operator $\mathbf{C}_2$ can be handled similarly and yields an identical expression. The common form is given by

$$\mathbf{C}(\mathbf{E}_{\rm T}) = i \sum_{n=-\infty}^{\infty} \frac{\exp(i\lambda_n x)}{\tilde{\mu}_n} \begin{bmatrix} \alpha_n n_{\rm r}^2 k^2 E_{nx} \\ \\ \beta_n \tilde{\mu}_n^2 E_{nz} \end{bmatrix}, \tag{29}$$

where

$$\begin{aligned}\alpha_n &= \frac{(n_{\mathrm{r}}^2\mu_n - \tilde{\mu}_n)\exp(i\tilde{\mu}_n a) - (n_{\mathrm{r}}^2\mu_n + \tilde{\mu}_n)\exp(-i\tilde{\mu}_n a)}{(n_{\mathrm{r}}^2\mu_n - \tilde{\mu}_n)\exp(i\tilde{\mu}_n a) + (n_{\mathrm{r}}^2\mu_n + \tilde{\mu}_n)\exp(-i\tilde{\mu}_n a)},\\ \beta_n &= \frac{(\tilde{\mu}_n - \mu_n)\exp(i\tilde{\mu}_n a) - (\tilde{\mu}_n + \mu_n)\exp(-i\tilde{\mu}_n a)}{(\tilde{\mu}_n - \mu_n)\exp(i\tilde{\mu}_n a) + (\tilde{\mu}_n + \mu_n)\exp(-i\tilde{\mu}_n a)}.\end{aligned} \tag{30}$$

Here

$$\tilde{\mu}_n = \sqrt{n_{\mathrm{r}}^2 k^2 - \lambda_n^2}, \tag{31}$$

with the same convention as before for the value of the square root, and

$$\mathbf{E}_{n\mathrm{T}} = \frac{1}{2L}\int_{-L}^{L} \exp(-i\lambda_n x)\mathbf{E}_{\mathrm{T}}(x,0)\,\mathrm{d}x, \tag{32}$$

for the front, $\mathbf{C}_1(\mathbf{E}_{\mathrm{T}})$, and

$$\mathbf{E}_{n\mathrm{T}} = \frac{1}{2L}\int_{-L}^{L} \exp(-i\lambda_n x)\mathbf{E}_{\mathrm{T}}(x,d)\,\mathrm{d}x, \tag{33}$$

for the back, $\mathbf{C}_2(\mathbf{E}_{\mathrm{T}})$.

For the special case in which the refractive indices of the free space and substrates match identically (i.e., $n_{\mathrm{r}} = 1$ and $\tilde{\mu}_n = \mu_n$), these operators simplify to

$$\mathbf{C}(\mathbf{E}_{\mathrm{T}}) = -i\sum_{n=-\infty}^{\infty} \frac{\exp(i\lambda_n x)}{\mu_n} \begin{bmatrix} k^2 E_{nx} \\ \\ \mu_n^2 E_{nz} \end{bmatrix}. \tag{34}$$

This corresponds to the simplest model problem in which the fields essentially exit the liquid-crystal film directly to the exterior free space. Operators of such forms as these in general are referred to as "exact radiation boundary conditions via eigenfunction expansions.[17]"

In general, whenever the front and back components consist of individual elements that are each uniform in x, then the admittance maps on pure modes will uncouple

and will be expressible in the form

$$\mathbf{C}_\alpha\big(\exp(i\lambda_n x)\mathbf{E}_\mathrm{T}\big) = \exp(i\lambda_n x) M_{\alpha n}\mathbf{E}_\mathrm{T}, \quad \alpha = 1, 2, \tag{35}$$

where $M_{\alpha n}$ are 2×2 matrices. For example, for the case above of a single glass substrate, we have

$$\begin{aligned}\mathbf{C}\big(\exp(i\lambda_n x)\mathbf{E}_\mathrm{T}\big) &= i\frac{\exp(i\lambda_n x)}{\tilde{\mu}_n}\begin{bmatrix} \alpha_n n_\mathrm{r}^2 k^2 E_x \\ \\ \beta_n \tilde{\mu}_n^2 E_z \end{bmatrix} \\ &= \exp(i\lambda_n x)\begin{bmatrix} i\alpha_n n_\mathrm{r}^2 k^2/\tilde{\mu}_n & 0 \\ \\ 0 & i\beta_n\tilde{\mu}_n \end{bmatrix}\mathbf{E}_\mathrm{T}, \end{aligned} \tag{36}$$

from which follows

$$M_{1n} = M_{2n} = \begin{bmatrix} i\alpha_n n_\mathrm{r}^2 k^2/\tilde{\mu}_n & 0 \\ \\ 0 & i\beta_n\tilde{\mu}_n \end{bmatrix}, \tag{37}$$

or, for the special case $n_\mathrm{r} = 1$, $\tilde{\mu}_n = \mu_n$,

$$M_{1n} = M_{2n} = \begin{bmatrix} -ik^2/\mu_n & 0 \\ \\ 0 & -i\mu_n \end{bmatrix}. \tag{38}$$

Anisotropic elements in the front or back components could lead to couplings between the x and z components of the modes ($M_{xz}^{\alpha n} \neq 0$ and/or $M_{zx}^{\alpha n} \neq 0$ above).

It is cases such as these in general, where the admittance maps are completely characterized by the 2×2 matrices $\{M_{1n}, M_{2n}\}_{n=-\infty}^{\infty}$, with which we can deal most effectively by our approach. In a similar way, we can construct an analytical formula for the equivalent surface current associated with incidence through a single glass lower substrate, which we do next.

C. *Equivalent Surface Current for Glass Substrates*

Also derived in Appendix A is the expression for the external field $\mathbf{E}_3$ associated with the equivalent surface current $\mathbf{g}_1$ for the case of a device as above with front components consisting only of a single glass substrate (of thickness a and index of refraction n_r). From it we can calculate the value of $\mathbf{g}_1$ using Eq. (21):

$$\mathbf{g}_{1\mathrm{T}}(x) = -4i \exp(ik_x x) \begin{bmatrix} \dfrac{n_\mathrm{r}^2 k^2 \exp(-ik_y a) E_{0x}^{\mathrm{inc}}}{(n_\mathrm{r}^2 k_y - \tilde{k}_y)\exp(i\tilde{k}_y a) + (n_\mathrm{r}^2 k_y + \tilde{k}_y)\exp(-i\tilde{k}_y a)} \\ \dfrac{k_y \tilde{k}_y \exp(-ik_y a) E_{0z}^{\mathrm{inc}}}{(\tilde{k}_y - k_y)\exp(i\tilde{k}_y a) + (\tilde{k}_y + k_y)\exp(-i\tilde{k}_y a)} \end{bmatrix}, \quad (39)$$

where $\mathbf{E}_{\mathrm{inc}}$ is characterized in Eqs. (9) and (10), with incident wave vector $(k_x, k_y, 0)$, and $\tilde{k}_y = (n_\mathrm{r}^2 k^2 - k_x^2)^{1/2}$ (the y component of the associated wave vector in the glass substrate). For the special (idealized) case of a transparent substrate ($n_\mathrm{r} = 1$, $\tilde{k}_y = k_y$, as before), this expression simplifies to

$$\mathbf{g}_{1\mathrm{T}}(x) = -\frac{2i}{k_y} \exp(ik_x x) \begin{bmatrix} k^2 E_{0x}^{\mathrm{inc}} \\ k_y^2 E_{0z}^{\mathrm{inc}} \end{bmatrix}. \quad (40)$$

Even in situations where the admittance maps and equivalent surface current cannot be worked out in terms of simple analytical formulas such as Eqs. (29) and (39), it would be expected that they could be calculated numerically without significant difficulty.

5. NUMERICAL DISCRETIZATION

The numerical modeling of a mathematical problem such as this has two main aspects: *discretization* and *solution*. The first replaces the continuum model with an approximate, discretized model containing a finite number of degrees of freedom. The

discretized model for our problem will be a large system of complex linear algebraic equations. The second part of the solution process consists of solving this system of equations numerically to determine these unknowns. We discuss these distinct aspects in this and the following section.

A. Finite-Element Discretization

The discretization of formulations of the Maxwell equations requires care. For a problem such as ours, the traditional approaches are *finite differences*, *finite elements*, or *spectral methods*. Finite-difference methods are well developed in certain areas of computational electromagnetics. They are generally applied to time-dependent formulations, where the approach goes by the name of the "Finite Difference Time Domain" (FDTD) method.[25] The application of this approach in our area (high-frequency propagation in inhomogeneous, anisotropic media) is relatively recent.[8–13]

A spectral approach in the context of a problem such as ours would take advantage of the quasi-periodicity of the fields in the x direction and would effectively seek approximate solutions in the form of truncated expansions of the general form

$$\mathbf{E}_h(x,y) = \sum_n \exp(i\lambda_n x)\mathbf{E}_n(y). \tag{41}$$

Such an ansatz leads to a coupled system of ordinary differential equations (or a weak formulation of such) for the unknown amplitude functions $\mathbf{E}_n(y)$; this system then requires further discretization and solution. In the special case of a relative dielectric tensor that is uniform in x (i.e., $\boldsymbol{\epsilon}_{\mathrm{r}}(x,y) = \boldsymbol{\epsilon}_{\mathrm{r}}(y)$), these equations become *uncoupled*—the problem is essentially one-dimensional in that case—and we exploit this below in Sec. 6B.

An advantage of a spectral method is that it requires many fewer degrees of freedom for the x dependence than the finite-difference and finite-element discretizations, which require a sufficiently large number of grid points or mesh cells per wavelength to resolve the fields accurately. A disadvantage of such an approach is that the resulting discretization matrix, though smaller, is less "sparse," that is, it contains relatively more non-zero elements and thus requires more computer memory to store and more work to solve in general (than a sparser linear system of comparable size).

The numerical modeling on which we report here utilizes a finite-element discretization (which we shall also interpret as equivalent finite-difference equations). In recent years, the numerical analysis community has devoted much attention to finite-element methods for such problems (see Ref. 26 for a recent review). There are subtleties that render standard element functions inappropriate for our formulation, and specialized elements must be used instead. The elements we use are referred to by various names: "Nédélec elements," "curl-conforming elements," "edge elements," "discrete Whitney forms." We have used the lowest-order such element for rectangular mesh cells: "constant tangential/linear normal" (CT/LN).[17,26]

We use a rectangular mesh on the computational domain $\Omega = (-L, L) \times (0, d)$ consisting of uniform cells in x and in y:

$$\begin{aligned} x_i &= i\Delta x, \qquad i = -I, \ldots, I, \quad \Delta x = \frac{L}{I}, \\ y_j &= j\Delta y, \qquad j = 0, \ldots, J, \quad \Delta y = \frac{d}{J}. \end{aligned} \tag{42}$$

An individual mesh cell, $(x_i, x_{i+1}) \times (y_j, y_{j+1})$, and associated local degrees of freedom are shown in Fig. 2. The approximate solution is represented locally in terms of the

degrees of freedom indicated there by the following formulas:

$$\begin{aligned}
E^h_x(x,y) &= E^x_{i+\frac{1}{2},j}\frac{y_{j+1}-y}{\Delta y} + E^x_{i+\frac{1}{2},j+1}\frac{y-y_j}{\Delta y},\\
E^h_y(x,y) &= E^y_{i,j+\frac{1}{2}}\frac{x_{i+1}-x}{\Delta x} + E^y_{i+1,j+\frac{1}{2}}\frac{x-x_i}{\Delta x},\\
E^h_z(x,y) &= E^z_{i,j}\frac{x_{i+1}-x}{\Delta x}\frac{y_{j+1}-y}{\Delta y} + E^z_{i+1,j}\frac{x-x_i}{\Delta x}\frac{y_{j+1}-y}{\Delta y}\\
&\quad + E^z_{i,j+1}\frac{x_{i+1}-x}{\Delta x}\frac{y-y_j}{\Delta y} + E^z_{i+1,j+1}\frac{x-x_i}{\Delta x}\frac{y-y_j}{\Delta y}.
\end{aligned} \tag{43}$$

Thus locally the E_x components are constant in x and linear in y, the E_y components are linear in x and constant in y, and the E_z components are bilinear in (x,y).

The global approximate vector fields are pieced together from these. The continuity properties of the components of $\mathbf{E}_h$ are consistent with the interface conditions that would correspond to the treatment of the dielectric tensor as piecewise constant (i.e., as a piecewise homogeneous but anisotropic medium): tangential components are continuous across horizontal and vertical mesh-cell interfaces, while normal components may have jumps. Even though E_x and E_y are not necessarily globally continuous, the resulting vector field does have finite energy (square-integrable curl). The global degrees of freedom then are, for $i = -I, \ldots, I-1$,

$$\begin{aligned}
&E^x_{i+\frac{1}{2},j}, \quad && j = 0,\ldots,J,\\
&E^y_{i,j+\frac{1}{2}}, && j = 0,\ldots,J-1,\\
&E^z_{i,j}, && j = 0,\ldots,J,
\end{aligned} \tag{44}$$

with $E^y_{I,*}$ and $E^z_{I,*}$ determined by the Floquet-Bloch conditions (11):

$$\begin{aligned}
E^y_{I,j+\frac{1}{2}} &= \exp(i2k_xL)E^y_{-I,j+\frac{1}{2}}, \quad j = 0,\ldots,J-1,\\
E^z_{I,j} &= \exp(i2k_xL)E^z_{-I,j}, \quad j = 0,\ldots,J.
\end{aligned} \tag{45}$$

These are depicted in Fig. 3.

The test fields $\mathbf{F}$ are approximated locally by the same formulas, Eqs. (43), and their values along the right boundary $x = L$ $(i = I)$ are determined in a similar way by the complementary Floquet-Bloch conditions (14). The computational problem that we must solve is obtained by substituting the local approximations for $\mathbf{E}$ and $\mathbf{F}$ into the weak formulation of the problem, Eq. (22), utilizing appropriate numerical quadrature for the integrals that cannot be computed exactly, and discretizing the admittance maps $\mathbf{C}_1$ and $\mathbf{C}_2$ in some appropriate way. We discuss these issues below. What results is a large sparse complex linear-algebraic system of equations

$$A\mathbf{e} = \mathbf{b}, \tag{46}$$

where the vector $\mathbf{e}$ contains the global degrees of freedom in some order. The total number of unknowns is $2I(3J + 2)$.

B. Equivalent Finite-Difference Equations

It is possible to interpret the discrete model as a system of finite-difference equations, and we do that now. We consider a slightly more general problem, with additional current sources, which will be needed in Sec. 6B below. Thus we augment the conjugate-linear form in Eq. (24)

$$l(\mathbf{F}) = \int_{\Gamma_1} \mathbf{g}_{1\mathrm{T}}(x) \cdot \mathbf{F}_{\mathrm{T}}^* + \int_{\Gamma_2} \mathbf{g}_{2\mathrm{T}}(x) \cdot \mathbf{F}_{\mathrm{T}}^* + \int_{\Omega} \mathbf{G}(x, y) \cdot \mathbf{F}^*. \tag{47}$$

The strong form of the associated system of partial differential equations can be written

$$\nabla \times (\nabla \times \mathbf{E}) - k^2 \mathbf{D} = \mathbf{G}(x, y), \quad \text{in } \Omega, \tag{48}$$

where we now use $\mathbf{D} = \boldsymbol{\epsilon}_{\rm r}(x,y)\mathbf{E}$ as a convenient notation, or in component form, for $-L < x < L$, $0 < y < d$,

$$\begin{aligned} \partial_y(\partial_x E_y - \partial_y E_x) - k^2 D_x &= G_x(x,y), \\ -\partial_x(\partial_x E_y - \partial_y E_x) - k^2 D_y &= G_y(x,y), \\ -\partial_x^2 E_z - \partial_y^2 E_z - k^2 D_z &= G_z(x,y), \end{aligned} \tag{49}$$

with non-local boundary conditions

$$\begin{aligned} [\hat{\mathbf{y}} \times (\nabla \times \mathbf{E})]_{\rm T} + \mathbf{C}_1(\mathbf{E}_{\rm T}) &= \mathbf{g}_{1\rm T}(x), \quad \text{on } \Gamma_1, \\ -[\hat{\mathbf{y}} \times (\nabla \times \mathbf{E})]_{\rm T} + \mathbf{C}_2(\mathbf{E}_{\rm T}) &= \mathbf{g}_{2\rm T}(x), \quad \text{on } \Gamma_2, \end{aligned} \tag{50}$$

or

$$\begin{aligned} (\partial_x E_y - \partial_y E_x)(x,0) + C_{1x}(x) &= g_{1x}(x), \\ -\partial_y E_z(x,0) + C_{1z}(x) &= g_{1z}(x), \end{aligned} \tag{51}$$

on $y = 0$, and

$$\begin{aligned} -(\partial_x E_y - \partial_y E_x)(x,d) + C_{2x}(x) &= g_{2x}(x), \\ \partial_y E_z(x,d) + C_{2z}(x) &= g_{2z}(x), \end{aligned} \tag{52}$$

on $y = d$, all valid for $-L < x < L$. In addition, the $\mathbf{E}$ field must still satisfy the quasi-periodicity conditions (11) and (12).

In our present implementation, for the numerical approximation of the integrals in Eqs. (23) and (24), we have approximated the relative dielectric tensor piecewise uniformly,

$$\boldsymbol{\epsilon}_{\rm r}(x,y) \approx \boldsymbol{\epsilon}_{\rm r}(x_{i+\frac{1}{2}}, y_{j+\frac{1}{2}}), \qquad x_i < x < x_{i+1}, \quad y_j < y < y_{j+1}, \tag{53}$$

and have employed a nodal quadrature rule,

$$\int_{y_j}^{y_{j+1}} \int_{x_i}^{x_{i+1}} f(x,y)\,\mathrm{d}x\,\mathrm{d}y \approx \frac{\Delta x \Delta y}{4}\left(f_{i,j} + f_{i+1,j} + f_{i,j+1} + f_{i+1,j+1}\right), \tag{54}$$

for the element area integrals and a composite trapezoidal rule for the boundary integrals. We utilize standard notation for centered finite-difference operators:

$$\delta_x u_i = \frac{u_{i+\frac{1}{2}} - u_{i-\frac{1}{2}}}{\Delta x}, \qquad \delta_x^2 u_i = \delta_x(\delta_x u_i) = \frac{u_{i+1} - 2u_i + u_{i-1}}{\Delta x^2}. \tag{55}$$

Our discretized equations can be written in the following form. For $i = -I, \ldots, I-1$,

$$\delta_y(\delta_x E^y_{i+\frac{1}{2},j} - \delta_y E^x_{i+\frac{1}{2},j}) - k^2 \overline{D}^x_{i+\frac{1}{2},j} = G^x_{i+\frac{1}{2},j}, \quad j = 1, \ldots, J-1, \tag{56a}$$

$$-\delta_x(\delta_x E^y_{i,j+\frac{1}{2}} - \delta_y E^x_{i,j+\frac{1}{2}}) - k^2 \overline{D}^y_{i,j+\frac{1}{2}} = G^y_{i,j+\frac{1}{2}}, \quad j = 0, \ldots, J-1, \tag{56b}$$

$$-\delta_x^2 E^z_{i,j} - \delta_y^2 E^z_{i,j} - k^2 \overline{D}^z_{i,j} = G^z_{i,j}, \quad j = 1, \ldots, J-1, \tag{56c}$$

where the components of $\mathbf{D}$ are approximated by the averages

$$\begin{aligned}
\overline{D}^x_{i+\frac{1}{2},j} = {} & \frac{\epsilon^{xx}_{i+\frac{1}{2},j-\frac{1}{2}} + \epsilon^{xx}_{i+\frac{1}{2},j+\frac{1}{2}}}{2} E^x_{i+\frac{1}{2},j} + \frac{1}{2}\left[\epsilon^{xy}_{i+\frac{1}{2},j-\frac{1}{2}} \frac{E^y_{i,j-\frac{1}{2}} + E^y_{i+1,j-\frac{1}{2}}}{2}\right. \\
& \left. + \epsilon^{xy}_{i+\frac{1}{2},j+\frac{1}{2}} \frac{E^y_{i,j+\frac{1}{2}} + E^y_{i+1,j+\frac{1}{2}}}{2}\right] + \frac{\epsilon^{xz}_{i+\frac{1}{2},j-\frac{1}{2}} + \epsilon^{xz}_{i+\frac{1}{2},j+\frac{1}{2}}}{2} \frac{E^z_{i,j} + E^z_{i+1,j}}{2},
\end{aligned}$$

$$\begin{aligned}
\overline{D}^y_{i,j+\frac{1}{2}} = {} & \frac{1}{2}\left[\epsilon^{yx}_{i-\frac{1}{2},j+\frac{1}{2}} \frac{E^x_{i-\frac{1}{2},j} + E^x_{i-\frac{1}{2},j+1}}{2} + \epsilon^{yx}_{i+\frac{1}{2},j+\frac{1}{2}} \frac{E^x_{i+\frac{1}{2},j} + E^x_{i+\frac{1}{2},j+1}}{2}\right] \\
& + \frac{\epsilon^{yy}_{i-\frac{1}{2},j+\frac{1}{2}} + \epsilon^{yy}_{i+\frac{1}{2},j+\frac{1}{2}}}{2} E^y_{i,j+\frac{1}{2}} + \frac{\epsilon^{yz}_{i-\frac{1}{2},j+\frac{1}{2}} + \epsilon^{yz}_{i+\frac{1}{2},j+\frac{1}{2}}}{2} \frac{E^z_{i,j} + E^z_{i,j+1}}{2},
\end{aligned} \tag{57}$$

$$\begin{aligned}
\overline{D}^z_{i,j} = {} & \frac{1}{2}\left[\frac{\epsilon^{zx}_{i-\frac{1}{2},j-\frac{1}{2}} + \epsilon^{zx}_{i-\frac{1}{2},j+\frac{1}{2}}}{2} E^x_{i-\frac{1}{2},j} + \frac{\epsilon^{zx}_{i+\frac{1}{2},j-\frac{1}{2}} + \epsilon^{zx}_{i+\frac{1}{2},j+\frac{1}{2}}}{2} E^x_{i+\frac{1}{2},j}\right] \\
& + \frac{1}{2}\left[\frac{\epsilon^{zy}_{i-\frac{1}{2},j-\frac{1}{2}} + \epsilon^{zy}_{i+\frac{1}{2},j-\frac{1}{2}}}{2} E^y_{i,j-\frac{1}{2}} + \frac{\epsilon^{zy}_{i-\frac{1}{2},j+\frac{1}{2}} + \epsilon^{zy}_{i+\frac{1}{2},j+\frac{1}{2}}}{2} E^y_{i,j+\frac{1}{2}}\right] \\
& + \frac{\epsilon^{zz}_{i-\frac{1}{2},j-\frac{1}{2}} + \epsilon^{zz}_{i+\frac{1}{2},j-\frac{1}{2}} + \epsilon^{zz}_{i-\frac{1}{2},j+\frac{1}{2}} + \epsilon^{zz}_{i+\frac{1}{2},j+\frac{1}{2}}}{4} E^z_{i,j}.
\end{aligned}$$

The difference equations (56) bear a clear formal relationship to the partial differential equations (49) and give second-order accurate approximations to them in the sense that the truncation error (consistency error) is formally $O(\Delta x^2 + \Delta y^2)$, which is in fact the rate of convergence we observe. Other types of quadrature rules and ways of approximating the dielectric tensor could produce different formulas for the averages in Eqs. (57). The piecewise-uniform approximation to $\boldsymbol{\epsilon}_{\mathrm{r}}(x, y)$, Eq. (53), is useful if there are internal interfaces in the film layer Ω, such as electrode strips, for example.

The first and last finite-difference equations for the x and z components contain contributions from the surface integrals:

$$\begin{aligned} \left(\delta_x E^y_{i+\frac{1}{2},\frac{1}{2}} - \delta_y E^x_{i+\frac{1}{2},\frac{1}{2}}\right) + C^{1x}_{i+\frac{1}{2}} &= g^{1x}_{i+\frac{1}{2}} + \frac{\Delta y}{2}\left(k^2 \overline{D}^x_{i+\frac{1}{2},0} + G^x_{i+\frac{1}{2},0}\right), \\ -\delta_y E^z_{i,\frac{1}{2}} + C^{1z}_i &= g^{1z}_i + \frac{\Delta y}{2}\left(\delta_x^2 E^z_{i,0} + k^2 \overline{D}^z_{i,0} + G^z_{i,0}\right), \end{aligned} \tag{58}$$

for $j = 0$, and

$$\begin{aligned} -\left(\delta_x E^y_{i+\frac{1}{2},J-\frac{1}{2}} - \delta_y E^x_{i+\frac{1}{2},J-\frac{1}{2}}\right) + C^{2x}_{i+\frac{1}{2}} &= g^{2x}_{i+\frac{1}{2}} + \frac{\Delta y}{2}\left(k^2 \overline{D}^x_{i+\frac{1}{2},J} + G^x_{i+\frac{1}{2},J}\right), \\ \delta_y E^z_{i,J-\frac{1}{2}} + C^{2z}_i &= g^{2z}_i + \frac{\Delta y}{2}\left(\delta_x^2 E^z_{i,J} + k^2 \overline{D}^z_{i,J} + G^z_{i,J}\right), \end{aligned} \tag{59}$$

for $j = J$. These give second-order accurate approximations to the non-local boundary conditions (51) and (52) and can be constructed in an alternate way by directly applying the method of "fictitious points" to Eqs. (51) and (52), that is, by introducing auxiliary grid points *outside* the domain, approximating the boundary conditions by symmetric finite-difference formulas involving these "fictitious points," and then using the difference equations for the x and z components from Eqs. (56) evaluated on the

boundaries (i.e., Eqs. (56a) and (56c), for $j = 0$ and $j = J$) to eliminate the fictitious degrees of freedom. See for example Sec. 2.13 of Ref. 27. The averages for $\mathbf{D}$ must be appropriately modified for these boundary grid cells:

$$\begin{aligned}
\overline{D}^x_{i+\frac{1}{2},0} &= \epsilon^{xx}_{i+\frac{1}{2},\frac{1}{2}} E^x_{i+\frac{1}{2},0} + \epsilon^{xy}_{i+\frac{1}{2},\frac{1}{2}} \frac{E^y_{i,\frac{1}{2}} + E^y_{i+1,\frac{1}{2}}}{2} + \epsilon^{xz}_{i+\frac{1}{2},\frac{1}{2}} \frac{E^z_{i,0} + E^z_{i+1,0}}{2}, \\
\overline{D}^z_{i,0} &= \frac{1}{2} \left[\epsilon^{zx}_{i-\frac{1}{2},\frac{1}{2}} E^x_{i-\frac{1}{2},0} + \epsilon^{zx}_{i+\frac{1}{2},\frac{1}{2}} E^x_{i+\frac{1}{2},0} \right] \\
&\quad + \frac{\epsilon^{zy}_{i-\frac{1}{2},\frac{1}{2}} + \epsilon^{zy}_{i+\frac{1}{2},\frac{1}{2}}}{2} E^y_{i,\frac{1}{2}} + \frac{\epsilon^{zz}_{i-\frac{1}{2},\frac{1}{2}} + \epsilon^{zz}_{i+\frac{1}{2},\frac{1}{2}}}{2} E^z_{i,0},
\end{aligned} \tag{60}$$

for $j = 0$, and

$$\begin{aligned}
\overline{D}^x_{i+\frac{1}{2},J} &= \epsilon^{xx}_{i+\frac{1}{2},J-\frac{1}{2}} E^x_{i+\frac{1}{2},J} + \epsilon^{xy}_{i+\frac{1}{2},J-\frac{1}{2}} \frac{E^y_{i,J-\frac{1}{2}} + E^y_{i+1,J-\frac{1}{2}}}{2} + \epsilon^{xz}_{i+\frac{1}{2},J-\frac{1}{2}} \frac{E^z_{i,J} + E^z_{i+1,J}}{2}, \\
\overline{D}^z_{i,J} &= \frac{1}{2} \left[\epsilon^{zx}_{i-\frac{1}{2},J-\frac{1}{2}} E^x_{i-\frac{1}{2},J} + \epsilon^{zx}_{i+\frac{1}{2},J-\frac{1}{2}} E^x_{i+\frac{1}{2},J} \right] \\
&\quad + \frac{\epsilon^{zy}_{i-\frac{1}{2},J-\frac{1}{2}} + \epsilon^{zy}_{i+\frac{1}{2},J-\frac{1}{2}}}{2} E^y_{i,J-\frac{1}{2}} + \frac{\epsilon^{zz}_{i-\frac{1}{2},J-\frac{1}{2}} + \epsilon^{zz}_{i+\frac{1}{2},J-\frac{1}{2}}}{2} E^z_{i,J},
\end{aligned} \tag{61}$$

for $j = J$.

As we can see, once an appropriate definition and staggering is given for the discrete unknowns—in this case, identical to the spatial part of the familiar Yee scheme utilized in time-domain calculations[28]—one can easily derive natural, symmetric, centered difference schemes directly from the partial differential equations and boundary conditions. Both of the equivalent points of view (finite elements and finite differences) are useful. We have relied upon the finite-element formulation for the coding and implementation of the assembly of the A matrix and b vector, while we have found the equivalent finite-difference equations more convenient for developing the numerical preconditioners, which accelerate the convergence of the iterative numerical solution algorithms and which we discuss in Sec. 6B.

C. Discrete Floquet Transforms and Discrete Admittance Maps

Under discretization, one deals with grid functions, which have finite Rayleigh series expansions determined by interpolation conditions (or discrete orthogonality conditions) rather than by integral formulas. The global degrees of freedom (44) can be expanded in terms of these, for $l = -I, \ldots, I-1$,

$$\begin{aligned} E^x_{l+\frac{1}{2},m} &= \sum_{n=-I}^{I-1} \widehat{E}^x_{n,m} \exp(i\lambda_n x_{l+\frac{1}{2}}), \quad m = 0, \ldots, J, \\ E^y_{l,m+\frac{1}{2}} &= \sum_{n=-I}^{I-1} \widehat{E}^y_{n,m+\frac{1}{2}} \exp(i\lambda_n x_l), \quad m = 0, \ldots, J-1, \\ E^z_{l,m} &= \sum_{n=-I}^{I-1} \widehat{E}^z_{n,m} \exp(i\lambda_n x_l), \quad m = 0, \ldots, J, \end{aligned} \tag{62}$$

where the discrete modal amplitudes are given by, for $n = -I, \ldots, I-1$,

$$\begin{aligned} \widehat{E}^x_{n,m} &= \frac{1}{2I} \sum_{l=-I}^{I-1} E^x_{l+\frac{1}{2},m} \exp(-i\lambda_n x_{l+\frac{1}{2}}), \quad m = 0, \ldots, J, \\ \widehat{E}^y_{n,m+\frac{1}{2}} &= \frac{1}{2I} \sum_{l=-I}^{I-1} E^y_{l,m+\frac{1}{2}} \exp(-i\lambda_n x_l), \quad m = 0, \ldots, J-1, \\ \widehat{E}^z_{n,m} &= \frac{1}{2I} \sum_{l=-I}^{I-1} E^z_{l,m} \exp(-i\lambda_n x_l), \quad m = 0, \ldots, J. \end{aligned} \tag{63}$$

These are sometimes referred to as the "discrete Floquet inverse transform" and "discrete Floquet transform" respectively. Since $\lambda_n = k_x + n\pi/L$, these differ only by pre-/post-scaling factors from the ordinary discrete Fourier inverse transform and transform and can thus be evaluated in $O(I \log I)$ work via fast Fourier transforms.

The discrete Floquet transforms can be used to construct discretizations of the admittance maps $\mathbf{C}_1$ and $\mathbf{C}_2$ in the cases where the front and back components are uniform in x, in which case $\mathbf{C}_1$ and $\mathbf{C}_2$ are completely characterized by the family of 2×2 matrices $\{M_{1n}, M_{2n}\}$ of Eq. (35). The discrete operators then will take as input the

degrees of freedom on the interfaces, $\{E^x_{i+\frac{1}{2},0}, E^z_{i,0}\}_{i=-I}^{I-1}$ on Γ_1 and $\{E^x_{i+\frac{1}{2},J}, E^z_{i,J}\}_{i=-I}^{I-1}$ on Γ_2 respectively, transform them using discrete Floquet transforms, apply M_{1n} and M_{2n} to the finite number of modal amplitudes ($n = -I, \ldots, I-1$), and transform back with inverse discrete Floquet transforms. This is a natural approach and exhibits 2nd-order pointwise accuracy at the nodes and edge centers. It differs a little from the approach of Ref. 14, which views the finite-element solution $\mathbf{E}_h$ from a continuum perspective and uses instead truncation of the infinite, continuous Rayleigh series expansions.

If some element of the front or back components fails to be uniform in x, then the outer problems for the $\mathbf{E}_1$, $\mathbf{E}_2$, and $\mathbf{E}_3$ fields do not all uncouple under the modal transforms, and the admittance maps cannot be characterized so simply. In such cases, our basic approach remains valid, however we will not be able to utilize the preconditioners discussed in the next section. Sometimes this difficulty can be overcome by including the offending parts of the front or back components in the definition of the domain Ω (which is treated as being completely inhomogeneous).

The discretized admittance maps are ultimately linear transformations on the grid functions $\{E^x_{i+\frac{1}{2},0}, E^z_{i,0}\}_{i=-I}^{I-1}$ and $\{E^x_{i+\frac{1}{2},J}, E^z_{i,J}\}_{i=-I}^{I-1}$ to $\{C^{1x}_{i+\frac{1}{2}}, C^{1z}_i\}_{i=-I}^{I-1}$ and $\{C^{2x}_{i+\frac{1}{2}}, C^{2z}_i\}_{i=-I}^{I-1}$ respectively. They can be represented in various ways, and we deal with them flexibly in our codes. Possible representations include (1) $4I \times 4I$ matrices (which represent the linear transformations via matrix-vector multiplication, with respect to some ordering of the grid values), (2) procedures or subroutines (which take as inputs the grid values of the discrete $\mathbf{E}$ field on Γ_1 and Γ_2 and return as outputs the grid values of the discretized $\mathbf{C}_1$ and $\mathbf{C}_2$), and (3) the collection of 2×2 matrices $\{M_{1n}, M_{2n}\}_{n=-I}^{I-1}$

(which represent the action of the operators on modal components, in the transform domain). The matrices of (1) are needed for the direct solution algorithms discussed below, while either (1) or (2) or (3) can be used for the basic iterative numerical solution procedures. Knowledge of representation (3) is required for the preconditioners, which rely on fast discrete Floquet transforms for speed of execution.

6. NUMERICAL SOLUTION

A. Discretization Matrix Structure and Solution Methods

The discretization matrix A of our system (46) is large, sparse, and complex, but it is *not* Hermitian. If k_x is complex (non-zero attenuation factor, $\kappa > 0$), then the Hermitian symmetry is destroyed by the Floquet-Bloch conditions (11) and (14). If k is real (no attenuation factor) and $\boldsymbol{\epsilon}_{\mathrm{r}}$ real symmetric (lossless, non-absorbing medium), then the contributions to A from the first terms of the $a(\cdot,\cdot)$ form, from Eq. (23),

$$\int_{\Omega} \{(\nabla \times \mathbf{E}) \cdot (\nabla \times \mathbf{F}^*) - k^2 [\boldsymbol{\epsilon}_{\mathrm{r}}(x,y)\mathbf{E}] \cdot \mathbf{F}^*\}, \tag{64}$$

will be Hermitian symmetric; however, the contributions from the admittance maps (boundary integrals) fail to be self-adjoint in general. For this one would require $\mathbf{C}^\dagger = \mathbf{C}$, where the adjoint linear operator is defined by

$$\int_{\Gamma} \mathbf{C}(\mathbf{E}_{\mathrm{T}}) \cdot \mathbf{F}_{\mathrm{T}}^* = \int_{\Gamma} \mathbf{E}_{\mathrm{T}} \cdot \mathbf{C}^\dagger(\mathbf{F}_{\mathrm{T}})^*, \tag{65}$$

to be valid for all admissible fields $\mathbf{E}$ and $\mathbf{F}$. For the idealized case of fields exiting the region Ω directly to an exterior free space, for example, we have from Eq. (34)

$$\mathbf{C}(\mathbf{E}_{\mathrm{T}}) = -i \sum_{n=-\infty}^{\infty} \frac{\exp(i\lambda_n x)}{\mu_n} \begin{bmatrix} k^2 E_{nx} \\ \\ \mu_n^2 E_{nz} \end{bmatrix}, \tag{66}$$

from which follows

$$\mathbf{C}^{\dagger}(\mathbf{F}_{\mathrm{T}}) = i \sum_{n=-\infty}^{\infty} \frac{\exp(i\lambda_n^* x)}{\mu_n^*} \begin{bmatrix} (k^*)^2 F_{nx} \\ (\mu_n^*)^2 F_{nz} \end{bmatrix}. \tag{67}$$

Even with k^2 and k_x real, in which case the evanescent-mode parts of $\mathbf{C}$ and $\mathbf{C}^{\dagger}$ (λ_n real, μ_n purely imaginary) agree, the propagating-mode parts (λ_n and μ_n real) differ by a factor of -1.

The linear system (46) can be solved by either *direct* or *iterative* methods. Direct solution requires assembling A and b, storing A in some sparse matrix format, and solving via a sparse, complex LU factorization and back solution. This is acceptable for problems in two spatial dimensions, such as ours, but would not be expected to be competitive for three-dimensional problems, to which we aspire. An alternate approach, essential in higher dimensions, would be to use an iterative algorithm, and we have implemented this as well in our code development.

Several possibilities exist for the iterative solution of systems such as ours, including GMRES (for which solid convergence analysis results are well established) and Orthomin (which has been utilized by Bao and Dobson[14] for diffractive optics calculations in other contexts). For our first implementation, the results from which are reported below, we have chosen to use Bi-CGSTAB, primarily because of its simplicity. This algorithm requires only the implementation of a matrix-vector product ($\mathbf{x} \mapsto A\mathbf{x}$) and (optionally) a "preconditioner" for A (see below). It does not require either of those functionalities for the Hermitian transpose $A^{\dagger}$, nor does it require any history vectors (and their associated extra storage). While it does not have as solid a convergence analysis as some of these other methods, it has performed acceptably

for our application. The actual algorithm is typical of such "Krylov Subspace Methods:" it is short, simple, and built upon matrix-vector multiplications, vector dot products, and short vector recurrences. Discussions of such methods can be found in Refs. 29–31.

Without an effective preconditioner, convergence of the Bi-CGSTAB iteration for our problem is unacceptably slow—see comparisons below. We are fortunate that there are very good preconditioners that can be implemented for our system. In general, preconditioning accelerates the convergence of iterative algorithms such as ours by effectively solving an equivalent problem of the form

$$M^{-1}A\mathbf{e} = M^{-1}\mathbf{b}. \tag{68}$$

Here the matrix M is the preconditioner, and the objective is to produce an equivalent problem for which the iterative algorithm converges much more rapidly. This can be accomplished if the preconditioned coefficient matrix is close to the identity matrix, $M^{-1}A \approx I$, or a scaling of it. The goal then is to construct an easily invertible preconditioner that achieves this. In physical applications, this is frequently done by constructing solution operators for discretizations of similar (but simpler) approximate problems, and we do this here next.

B. Preconditioning

For the purposes of constructing a preconditioner, it is necessary to consider a problem of the form

$$\begin{aligned} \nabla \times (\nabla \times \mathbf{E}) - k^2 \boldsymbol{\epsilon}_{\mathrm{r}}(x,y)\mathbf{E} &= \mathbf{G}(x,y), \quad \text{in } \Omega, \\ [\hat{\mathbf{y}} \times (\nabla \times \mathbf{E})]_{\mathrm{T}} + \mathbf{C}_1(\mathbf{E}_{\mathrm{T}}) &= \mathbf{0}, \quad \text{on } \Gamma_1, \\ -[\hat{\mathbf{y}} \times (\nabla \times \mathbf{E})]_{\mathrm{T}} + \mathbf{C}_2(\mathbf{E}_{\mathrm{T}}) &= \mathbf{0}, \quad \text{on } \Gamma_2, \end{aligned} \tag{69}$$

with a given current density $\mathbf{G}$ and subject to the same Floquet-Bloch conditions (11) and (12). In a preconditioning step, $\mathbf{G}$ will be related to the residual associated with the approximate solution vector at that stage of the iteration, and $\mathbf{E}$ will be related to the error (correction) between the current approximate solution and the true solution of the discrete problem. If the relative dielectric tensor were uniform in x, then our discretization of such a problem could be solved very efficiently using fast transforms—assuming that the external components of the device were all uniform in x as well.

We are thus led to consider approximate, preconditioning problems for which the dielectric tensor has been approximated by one that is uniform in x:

$$\boldsymbol{\epsilon}_{\mathrm{r}}(x,y) \approx \boldsymbol{\epsilon}_{\mathrm{p}}(y). \tag{70}$$

Two possibilities suggest themselves: a homogeneous, isotropic medium,

$$\boldsymbol{\epsilon}_{\mathrm{p}}(y) = n_{\mathrm{p}}^2 \boldsymbol{I}, \quad 0 < y < d, \tag{71}$$

where n_{p} is some (constant) effective index of refraction for the liquid-crystal layer,

or

$$\boldsymbol{\epsilon}_{\mathrm{p}}(y) = \frac{1}{2L}\int_{-L}^{L} \boldsymbol{\epsilon}_{\mathrm{r}}(x,y)\,\mathrm{d}x, \quad 0 < y < d, \tag{72}$$

in which the true relative dielectric tensor has been averaged in the lateral direction. In implementation, Eq. (71) is cleaner and faster per step, whereas Eq. (72) has more fidelity to the original problem but requires more work per step. We discuss the implementation of Eq. (71) but will report benchmarking results (in the next section) for Eq. (72).

From Eqs. (56), (58), and (59), we can obtain the finite-difference equations for the preconditioning problem under the assumption (71). They are given by, for $l = -I, \ldots, I-1$,

$$\begin{gathered}
\frac{2}{\Delta y}\left(\delta_x E^y_{l+\frac{1}{2},\frac{1}{2}} - \delta_y E^x_{l+\frac{1}{2},\frac{1}{2}}\right) - k^2 n_{\mathrm{p}}^2 E^x_{l+\frac{1}{2},0} + \frac{2}{\Delta y} C^{1x}_{l+\frac{1}{2}} = G^x_{l+\frac{1}{2},0}, \\
\delta_y\left(\delta_x E^y_{l+\frac{1}{2},m} - \delta_y E^x_{l+\frac{1}{2},m}\right) - k^2 n_{\mathrm{p}}^2 E^x_{l+\frac{1}{2},m} = G^x_{l+\frac{1}{2},m}, \quad m = 1, \ldots, J-1, \\
-\frac{2}{\Delta y}\left(\delta_x E^y_{l+\frac{1}{2},J-\frac{1}{2}} - \delta_y E^x_{l+\frac{1}{2},J-\frac{1}{2}}\right) - k^2 n_{\mathrm{p}}^2 E^x_{l+\frac{1}{2},J} + \frac{2}{\Delta y} C^{2x}_{l+\frac{1}{2}} = G^x_{l+\frac{1}{2},J},
\end{gathered} \tag{73}$$

$$-\delta_x\left(\delta_x E^y_{l,m+\frac{1}{2}} - \delta_y E^x_{l,m+\frac{1}{2}}\right) - k^2 n_{\mathrm{p}}^2 E^y_{l,m+\frac{1}{2}} = G^y_{l,m+\frac{1}{2}}, \quad m = 0, \ldots, J-1, \tag{74}$$

$$\begin{gathered}
-\delta_x^2 E^z_{l,0} - \frac{2}{\Delta y}\delta_y E^z_{l,\frac{1}{2}} - k^2 n_{\mathrm{p}}^2 E^z_{l,0} + \frac{2}{\Delta y} C^{1z}_{l} = G^z_{l,0}, \\
-\delta_x^2 E^z_{l,m} - \delta_y^2 E^z_{l,m} - k^2 n_{\mathrm{p}}^2 E^z_{l,m} = G^z_{l,m}, \quad m = 1, \ldots, J-1, \\
-\delta_x^2 E^z_{l,J} + \frac{2}{\Delta y}\delta_y E^z_{l,J-\frac{1}{2}} - k^2 n_{\mathrm{p}}^2 E^z_{l,J} + \frac{2}{\Delta y} C^{2z}_{l} = G^z_{l,J},
\end{gathered} \tag{75}$$

We solve by computing the discrete Floquet transforms of the right-hand-side current densities (residuals) using Eqs. (63), and seek solutions in terms of the modal

expansions (62). We make use of the formula

$$\delta_x \exp(i\lambda x) = \frac{\exp\big(i\lambda\left(x+\frac{\Delta x}{2}\right)\big) - \exp\big(i\lambda\left(x-\frac{\Delta x}{2}\right)\big)}{\Delta x} = \frac{2i}{\Delta x}\sin\left(\lambda\frac{\Delta x}{2}\right)\exp(i\lambda x). \tag{76}$$

We also make use of the relations

$$\begin{bmatrix} \widehat{C}_n^{1x} \\ \widehat{C}_n^{1z} \end{bmatrix} = \begin{bmatrix} M_{xx}^{1n} & M_{xz}^{1n} \\ M_{zx}^{1n} & M_{zz}^{1n} \end{bmatrix} \begin{bmatrix} \widehat{E}_{n,0}^{x} \\ \widehat{E}_{n,0}^{z} \end{bmatrix}, \quad \begin{bmatrix} \widehat{C}_n^{2x} \\ \widehat{C}_n^{2z} \end{bmatrix} = \begin{bmatrix} M_{xx}^{2n} & M_{xz}^{2n} \\ M_{zx}^{2n} & M_{zz}^{2n} \end{bmatrix} \begin{bmatrix} \widehat{E}_{n,J}^{x} \\ \widehat{E}_{n,J}^{z} \end{bmatrix}, \tag{77}$$

with the 2×2 matrices $\{M_{1n}, M_{2n}\}$ as given in Eq. (35).

We obtain the following system of uncoupled equations for the modal amplitudes:

for $n = -I, \ldots, I-1$,

$$\begin{aligned}
&\frac{2}{\Delta y}\left[\frac{2i}{\Delta x}\sin\left(\lambda_n\frac{\Delta x}{2}\right)\widehat{E}_{n,\frac{1}{2}}^{y} - \delta_y \widehat{E}_{n,\frac{1}{2}}^{x}\right] - k^2 n_{\mathrm{p}}^2 \widehat{E}_{n,0}^{x} \\
&\qquad + \frac{2}{\Delta y}\left(M_{xx}^{1n}\widehat{E}_{n,0}^{x} + M_{xz}^{1n}\widehat{E}_{n,0}^{z}\right) = \widehat{G}_{n,0}^{x}, \\
&\frac{2i}{\Delta x}\sin\left(\lambda_n\frac{\Delta x}{2}\right)\delta_y \widehat{E}_{n,m}^{y} - \delta_y^2 \widehat{E}_{n,m}^{x} - k^2 n_{\mathrm{p}}^2 \widehat{E}_{n,m}^{x} = \widehat{G}_{n,m}^{x}, \quad m = 1, \ldots, J-1, \\
&-\frac{2}{\Delta y}\left[\frac{2i}{\Delta x}\sin\left(\lambda_n\frac{\Delta x}{2}\right)\widehat{E}_{n,J-\frac{1}{2}}^{y} - \delta_y \widehat{E}_{n,J-\frac{1}{2}}^{x}\right] - k^2 n_{\mathrm{p}}^2 \widehat{E}_{n,J}^{x} \\
&\qquad + \frac{2}{\Delta y}\left(M_{xx}^{2n}\widehat{E}_{n,J}^{x} + M_{xz}^{2n}\widehat{E}_{n,J}^{z}\right) = \widehat{G}_{n,J}^{x},
\end{aligned} \tag{78}$$

$$\begin{aligned}
&\frac{4}{\Delta x^2}\sin^2\left(\lambda_n\frac{\Delta x}{2}\right)\widehat{E}_{n,m+\frac{1}{2}}^{y} + \frac{2i}{\Delta x}\sin\left(\lambda_n\frac{\Delta x}{2}\right)\delta_y \widehat{E}_{n,m+\frac{1}{2}}^{x} \\
&\qquad - k^2 n_{\mathrm{p}}^2 \widehat{E}_{n,m+\frac{1}{2}}^{y} = \widehat{G}_{n,m+\frac{1}{2}}^{y}, \quad m = 0, \ldots, J-1,
\end{aligned} \tag{79}$$

$$\frac{4}{\Delta x^2}\sin^2\left(\lambda_n\frac{\Delta x}{2}\right)\widehat{E}^z_{n,0}-\frac{2}{\Delta y}\delta_y\widehat{E}^z_{n,\frac{1}{2}}-k^2n_{\rm p}^2\widehat{E}^z_{n,0}$$
$$+\frac{2}{\Delta y}\left(M^{1n}_{zx}\widehat{E}^x_{n,0}+M^{1n}_{zz}\widehat{E}^z_{n,0}\right)=G^z_{n,0},$$
$$\frac{4}{\Delta x^2}\sin^2\left(\lambda_n\frac{\Delta x}{2}\right)\widehat{E}^z_{n,m}-\delta_y^2\widehat{E}^z_{n,m}-k^2n_{\rm p}^2\widehat{E}^z_{n,m}=\widehat{G}^z_{n,m},\quad m=1,\ldots,J-1, \tag{80}$$
$$\frac{4}{\Delta x^2}\sin^2\left(\lambda_n\frac{\Delta x}{2}\right)\widehat{E}^z_{n,J}+\frac{2}{\Delta y}\delta_y\widehat{E}^z_{n,J-\frac{1}{2}}-k^2n_{\rm p}^2\widehat{E}^z_{n,J}$$
$$+\frac{2}{\Delta y}\left(M^{2n}_{zx}\widehat{E}^x_{n,J}+M^{2n}_{zz}\widehat{E}^z_{n,J}\right)=\widehat{G}^z_{n,J}.$$

The resulting linear algebraic system of equations has $3J+2$ unknowns (for each n), and with the equations and unknowns properly ordered, it has a banded coefficient matrix with seven diagonals (three below and three above the main diagonal). It can be solved in $O(J)$ work by direct elimination. Thus the values for all the modal amplitudes, for $n=-I,\ldots,I-1$, can be computed in $O(IJ)$ work.

The preconditioning problem must be solved twice at each iteration of the Bi-CGSTAB solver. The vector to which the preconditioner solution matrix M^{-1} must be applied is related to the "residual" vector associated with the approximate solution vector at the current stage of the iteration, i.e., to the defect or amount by which that vector fails to solve the true problem: $\mathbf{r}_{\rm c}=\mathbf{b}-A\mathbf{e}_{\rm c}$. The entire solution of the discrete preconditioning problem proceeds in three stages: (1) performing discrete Floquet transforms with respect to x on the current residual vector to determine $\widehat{G}^x_{n,m}$, $\widehat{G}^z_{n,m}$, $m=0,\ldots,J$, and $\widehat{G}^y_{n,m+\frac{1}{2}}$, $m=0,\ldots,J-1$; (2) forming and solving the decoupled banded linear systems for $\widehat{E}^x_{n,m}$, $\widehat{E}^y_{n,m+\frac{1}{2}}$, and $\widehat{E}^z_{n,m}$ for each $n=-I,\ldots,I-1$; and (3) performing inverse discrete Floquet transforms of those solutions to reconstruct the components of the new vector, $E^x_{l+\frac{1}{2},m}$, $E^y_{l,m+\frac{1}{2}}$, and $E^z_{l,m}$. The total amount of

work is $O(IJ \log I)$, for a problem with $O(IJ)$ unknowns. In a typical problem, each preconditioned iteration improves the accuracy by roughly one decimal digit, and so the iterative solver only needs to execute on the order of 4–6 iterations. We describe some of these benchmarking aspects in the next section.

This type of preconditioning, via so-called "fast direct solvers," is common and is effective in situations such as ours. Variants of it have been used in other contexts involving diffractive optics calculations.[14] Our approach differs slightly from Ref. 14 in that we use fast transforms to solve directly the discrete preconditioning problem, Eqs. (73), (74), and (75), instead of formulating a continuous preconditioning problem in the transform domain and then discretizing it in some way that is compatible with the overall discretization of the original problem. We found the latter approach prone to ill conditioning of the uncoupled linear systems for the modal amplitudes associated with the high frequencies.

The action of the preconditioning matrix M^{-1} is essentially equivalent to that of a discrete Green's function, and in principle the same effect could be achieved by using a Green's function to convert the original problem to an equivalent integral equation formulation, discretizing, and solving the resulting (well conditioned) linear-algebraic system of equations by an unpreconditioned iterative algorithm with the matrix-vector multiplications realized by fast transforms. We have found our approach more convenient from an implementation point of view, as it allows for a flexible handling of the components of the device external to the film layer, which can be characterized independently and provided as a "user input." The approach also allows one to deal with preconditioning problems for which the effective/approximate relative dielectric

tensor $\boldsymbol{\epsilon}_{\mathrm{p}}(y)$ has a bona-fide y dependence, while for such problems in general it would not be possible to write down an analytical expression for the needed Green's functions.

The fast solution of our preconditioning problem relies on the decoupling of the problems for the individual modes, and this is lost if any external component (front or back) fails to be uniform in x. Any parts not uniform in x need to be encompassed in the computational domain Ω.

7. BENCHMARKING

Some tests were performed to gauge the accuracy and efficiency of the numerical approach. For this purpose, it is sufficient to use a simple model problem, with a known analytical solution. Thus we consider a film layer consisting of a slab of glass (homogeneous, isotropic) of index of refraction $n_{\mathrm{r}} = 1.5$ embedded in an exterior free space (i.e., no front or back components). The dimensions of Ω are chosen to be $d = L = 2\lambda_0/3$, where λ_0 is the free-space wavelength of the incident light, so that both d and L are equal to one wavelength of the light in the medium. The problem was discretized as described in Sec. 5.

Analytical solutions can be constructed easily, and so pointwise errors (at the nodes, for E_z, and at the horizontal and vertical edge centers, for E_x and E_y) can be computed. Representative results are presented in Table 1. The numerical data give clear indication of $O(h^2)$ accuracy: as the cell size $h = \Delta x = \Delta y$ is reduced by $\frac{1}{2}$, the maximum error is reduced by $\frac{1}{4}$. These and other tests lead to the rule of thumb that to obtain 5% pointwise error requires roughly 16 grid points per wavelength of light

in the medium, while to obtain 1% error, it is necessary to use about 32 grid points per wavelength.

We note that the published theoretical convergence analyses for discretizations of problems such as ours are of the typical finite-element nature: $O(h)$ errors with respect to energy norms, in $H(\mathrm{curl};\Omega)$, and $O(h^2)$ with respect to mean-square errors, $L^2(\Omega)$.[32] Some results in the direction of nodal convergence are indicated in Ref. 33, but with respect to somewhat different discrete norms. We are not aware of any rigorous analysis proving the second-order pointwise convergence that is clearly observed with our code using this established discretization method.

The complex linear algebraic system of equations was solved as described in Sec. 6, using the Bi-CGSTAB iterative algorithm, with or without preconditioning. The implementation was coded in Fortran 90 and tested on an older workstation with a 240 MHz PA-RISC processor, on which floating-point arithmetic is roughly comparable to that of a 500 MHz Pentium PC. The iterations were started from a zero initial guess and stopped at a maximum absolute error of 10^{-4}. Table 2 contains results for a representative problem.

The big improvement afforded by the preconditioner is clear, as are the scaling laws that govern work versus problem size. For the un-preconditioned calculations, when I and J are doubled (and the total number of unknowns quadrupled), the number of iterations increases by a factor of four, as does the problem size (and work per iteration), leading to an increase in total work and time by a factor of *sixteen*. This would be unacceptable even on a faster, more modern machine. The observed performance for the preconditioned calculations is consistent with the previously stated

work estimate of $O(IJ \log I)$: as I and J are doubled, the total work and time increase by a factor slightly greater than four.

The main storage requirements for the code come from the matrix A, stored in some sparse matrix format, the vector $\mathbf{e}$, which contains the current approximate solution, and a few auxiliary vectors of the same size that are required by the iterative algorithm, the total of which is proportional to the product IJ. Thus the largest problem that can be dealt with on a given platform by this approach is limited by the *area* of the computational domain Ω ($= 2dL$) and the wavelength of the light in the medium (since a certain number of grid points per wavelength are required to meet the desired accuracy needs). On a computer with 512 MB RAM, for a typical problem (light in the middle of the visible range, refractive indices of the order of 1.5), the maximum tractable domain size is roughly 100 μm^2 and takes on the order of 30 minutes to solve on our (older) workstation—the current class of personal computers can solve such a problem much faster.

8. APPLICATION

For the purposes of evaluation, we have used our techniques to analyze the reflection and transmission properties of an idealized IPS-mode ("In Plane Switching") liquid-crystal cell.[34,35] Such devices were originally introduced (with a different anchoring orientation) in Ref. 36. The primary advantage of the IPS mode is its improved optical performance at wide viewing angles. In particular, the IPS mode improves upon the poor grayscale performance that plagues the more conventional twisted-nematic mode used in most high-resolution liquid crystal display devices. A typical director field for

such a cell, in the "on state," is depicted in Fig. 4; in the off state, the directors would all be aligned uniformly in the vertical direction. This particular film is 5 μm thick and has a periodicity of 8 μm; these correspond to the actual dimensions of physical cells that were fabricated and experimentally characterized by Liu and Kelly[37] (see also Ref. 38).

The cell is illuminated from below by a normally incident monochromatic plane wave with a vacuum wavelength of 550 nm. The source is linearly polarized in the $\hat{\mathbf{x}}$ direction, and the ordinary and extra-ordinary refractive indices are taken to be $n_{\mathrm{o}} = 1.5$ and $n_{\mathrm{e}} = 1.6$. Results are included for two cases: no front/back external components vs idealized crossed polarizers ($\pm 45^{\circ}$). In order to compare with other numerical results, the influence of the confining glass substrates has been ignored—one would anticipate an error of the order of 5% as a consequence.

The wavelength of the light in the medium is around 350 nm; so the dimensions of the computational domain Ω in these units are about 23 by 14 wavelengths. We have used a grid of 1024×640 total grid cells ($I = 512$, $J = 640$), which gives approximately 45 grid points per wavelength in the medium. We estimate that this produces a discretization error of the order of a .5% in our calculated results.

Figures 5 give the intensity variations along the front and back interfaces, $y = 0$ and $y = 5$ μm, for the two cases (no polarizers vs crossed polarizers). They reflect the focusing and interference effects caused by the spatial variation of the director field (optic axis). In particular, considerable blockage of transmission is realized in the case of crossed polarizers near those regions where the director field is approximately uniform in the vertical direction ($x = \pm 4$ μm and, to a lesser degree, $x = 0$).

These systems were modeled numerically as well by Liu and Kelly using the Geometric Optics Approximation (GOA) and Beam Propagation Method (BPM). Their results are displayed in Figs. 6. Comparing those results to our high-accuracy approximations, we see that both of the approximate techniques (GOA and BPM) give qualitatively correct solutions in this context, with BPM doing an especially good job. This is to be expected, since this particular problem is very well suited to that method of approximation: the problem is planar, and reflections play a very small role. Our higher-resolution numerics contain finer detail and structure on a finer scale.

9. CONCLUSION

We have considered numerical modeling based upon the time-harmonic Maxwell equations (THM) to characterize the optical properties of 1-D-periodic 2-D devices with inhomogeneous and anisotropic dielectric properties. Our experience allows us to understand the intrinsic limitations of this type of approach and to make comparisons to other approaches.

Methods such as BPM and GOA introduce approximations at the mathematical level, whereas approaches such as ours (and the FDTD method as well) are discretizations of the *exact* mathematical model and, therefore, are in principle refinable to whatever accuracy your computing resources can accommodate. For problems to which BPM and GOA apply, those methods are more efficient than either of these "exact" approaches. BPM and GOA ignore reflections, however, and so they are not applicable to problems where these play a big role, as is the case, for example, with

reflective displays. Besides being applicable in settings where approximate methods such as BPM and GOA are not, refinable methods such as ours serve a useful purpose as benchmarking tools for these other methods.

Our approach also has certain advantages over the FDTD method. In the first place, it delivers time-harmonic quantities directly (which is a benefit when those are the quantities of interest) and does not require time averaging a steady state solution as FDTD would to obtain such values. In the same context, FDTD requires explicit time stepping (within a numerical stability restriction on the magnitude of the time step) to integrate numerically to steady state; whereas the THM approach affords different methods for solving the discretized problem, including *direct* numerical linear algebra or rapidly converging preconditioned *iterative* methods. The availability of such a good preconditioner will be especially valuable for problems in three spatial dimensions. A third advantage is that with the THM approach it is not necessary to introduce any grid points outside the single cell containing one period of the film layer—FDTD requires a truncated exterior grid with absorbing artificial boundary conditions and such.

There are some disadvantages to our approach. It is more complicated to implement (than BPM, GOA, or FDTD). As is the case with FDTD, it is a low-order discretization method, $O(\Delta x^2 + \Delta y^2)$, and so it requires 10's of grid points per wavelength in the medium to achieve acceptable spatial resolution of the electromagnetic field variables. As indicated previously, for typical applications, this limits us with our code to cell sizes on the order of 100 μm^2 in area.

Another disadvantage is that the problems for the exterior fields $\mathbf{E}_1$, $\mathbf{E}_2$, and $\mathbf{E}_3$,

which characterize the admittance maps $\mathbf{C}_1$ and $\mathbf{C}_2$ and the equivalent surface current $\mathbf{g}_1$, can be degenerate for certain angles of incidence even when the full problem is well posed (non-resonant). This can happen if the external components are lossless and the numerical attenuation coefficient κ is taken to be zero, in which case there can be "surface modes" for a finite set of angles of incidence. Using a positive κ easily removes this difficulty, and this parameter can be tuned so that the error introduced into the computed solution is below the level of the intrinsic numerical discretization error. If accurate answers are desired for such angles of incidence, they can be obtained either by extrapolation as $\kappa \to 0$ or by interpolation from well-posed calculations at nearby angles of incidence. Other approaches to closing the infinite-domain problem, such as using a larger computational domain truncated beyond all of the device components where artificial radiation boundary conditions are imposed, may not suffer from this—of course this comes at the cost of having to deal with a much larger computational domain and discrete system of equations.

For the exposition in this paper, we have limited ourselves to incidence in the x-y plane, but this is not an essential restriction. Problems with non-planar incidence ($k_z \neq 0$) can be handled in the same way and produce very similar systems with a few additional terms in the various integrals in the weak formulation, provided that material uniformity in the z direction is maintained and the field is sought in the form

$$\mathbf{E}(x, y, z) = \exp(ik_z z)\widetilde{\mathbf{E}}(x, y). \tag{81}$$

The restriction that is of a more fundamental nature is that of *periodicity* in one

direction. That is what enables the reduction of the computational problem to a single periodic cell, as well as makes it possible to construct a fast-direct preconditioner.

Many of the ideas utilized in our approach have come from other application areas. Our objective has been to adapt them to this context and to develop the new aspects necessary to make them effective here.

Acknowledgments

This research was supported in part by the National Science Foundation Science and Technology Center on "Advanced Liquid Crystalline Optical Materials" (ALCOM), DMR 89-20147. The work of the second author was also supported in part by NSF grants DMS-9870420 and DMS-0107761. A major portion of this work was developed in the thesis of the first author.[39] We are grateful to Peter Palffy-Muhoray (Liquid Crystal Institute, Kent State University) and Rolfe G. Petschek (Physics Department, Case Western Reserve University) for helpful discussions.

A. APPENDIX: OUTER SOLUTIONS $\mathbf{E}_1$, $\mathbf{E}_2$, AND $\mathbf{E}_3$ FOR SINGLE GLASS SUBSTRATE

In the case of a front component consisting of a single glass substrate, the external field $\mathbf{E}_1$ associated with the Calderon operator $\mathbf{C}_1$ satisfies

$$\begin{aligned} \nabla^2\mathbf{E}_1 + n_{\mathrm{r}}^2 k^2 \mathbf{E}_1 = \mathbf{0}, \quad \nabla\cdot\mathbf{E}_1 = 0, \qquad -a < y < 0, \\ \nabla^2\mathbf{E}_1 + k^2 \mathbf{E}_1 = \mathbf{0}, \quad \nabla\cdot\mathbf{E}_1 = 0, \qquad -\infty < y < -a, \end{aligned} \tag{82}$$

with boundary conditions specifying agreement with the total field on $y = 0$:

$$\mathbf{E}_{1\mathrm{T}}(x,0) = \mathbf{E}_{\mathrm{T}}(x,0), \quad -L < x < L. \tag{83}$$

It also satisfies the quasi-periodicity conditions, Eqs. (11) and (12), and the interface conditions (continuity of $\mathbf{E}_{1\mathrm{T}}$ and $(\nabla \times \mathbf{E}_1)_{\mathrm{T}}$ across $y = -a$), and it must be outward radiating as $y \to -\infty$. It can be represented in the form

$$\mathbf{E}_1(x,y) = \begin{cases} \displaystyle\sum_{n=-\infty}^{\infty} \exp(i\lambda_n x)[\exp(i\tilde{\mu}_n y)\mathbf{A}_n + \exp(-i\tilde{\mu}_n y)\mathbf{B}_n], & -a < y < 0 \\ \displaystyle\sum_{n=-\infty}^{\infty} \exp(i\lambda_n x)\exp[-i\mu_n(y+a)]\mathbf{C}_n, & -\infty < y < -a \end{cases} \tag{84}$$

where

$$\tilde{\mu}_n = \sqrt{n_{\mathrm{r}}^2 k^2 - \lambda_n^2}, \tag{85}$$

with the same convention as before for the value of the square root. The amplitudes $\mathbf{A}_n$, $\mathbf{B}_n$, and $\mathbf{C}_n$ are to be determined.

The boundary conditions give

$$\mathbf{E}_{1\mathrm{T}}(x,0) = \mathbf{E}_{\mathrm{T}}(x,0) = \sum_{n=-\infty}^{\infty} \exp(i\lambda_n x)\mathbf{E}_{n\mathrm{T}}, \tag{86}$$

where

$$\mathbf{E}_{n\mathrm{T}} = \frac{1}{2L}\int_{-L}^{L} \exp(-i\lambda_n x)\mathbf{E}_{\mathrm{T}}(x,0)\,\mathrm{d}x. \tag{87}$$

Using these, together with the continuity of $\mathbf{E}_{1\mathrm{T}}$ and $(\nabla \times \mathbf{E}_1)_{\mathrm{T}}$ across $y = -a$, plus the relations implied by Gauss's Law ($\nabla \cdot \mathbf{E}_1 = 0$), namely

$$\begin{aligned} \lambda_n A_{nx} + \tilde{\mu}_n A_{ny} &= 0, \\ \lambda_n B_{nx} - \tilde{\mu}_n B_{ny} &= 0, \\ \lambda_n C_{nx} - \mu_n C_{ny} &= 0, \end{aligned} \tag{88}$$

we obtain the following formulas for the components of the polarization vectors:

$$\begin{aligned}
A_{nx} &= \frac{(n_{\mathrm{r}}^2\mu_n - \tilde{\mu}_n)\exp(i\tilde{\mu}_n a)}{(n_{\mathrm{r}}^2\mu_n - \tilde{\mu}_n)\exp(i\tilde{\mu}_n a) + (n_{\mathrm{r}}^2\mu_n + \tilde{\mu}_n)\exp(-i\tilde{\mu}_n a)}E_{nx}, \\
B_{nx} &= \frac{(n_{\mathrm{r}}^2\mu_n + \tilde{\mu}_n)\exp(-i\tilde{\mu}_n a)}{(n_{\mathrm{r}}^2\mu_n - \tilde{\mu}_n)\exp(i\tilde{\mu}_n a) + (n_{\mathrm{r}}^2\mu_n + \tilde{\mu}_n)\exp(-i\tilde{\mu}_n a)}E_{nx}, \\
C_{nx} &= \frac{2n_{\mathrm{r}}^2\mu_n}{(n_{\mathrm{r}}^2\mu_n - \tilde{\mu}_n)\exp(i\tilde{\mu}_n a) + (n_{\mathrm{r}}^2\mu_n + \tilde{\mu}_n)\exp(-i\tilde{\mu}_n a)}E_{nx},
\end{aligned} \tag{89}$$

and

$$\begin{aligned}
A_{nz} &= \frac{(\tilde{\mu}_n - \mu_n)\exp(i\tilde{\mu}_n a)}{(\tilde{\mu}_n - \mu_n)\exp(i\tilde{\mu}_n a) + (\tilde{\mu}_n + \mu_n)\exp(-i\tilde{\mu}_n a)}E_{nz}, \\
B_{nz} &= \frac{(\tilde{\mu}_n + \mu_n)\exp(-i\tilde{\mu}_n a)}{(\tilde{\mu}_n - \mu_n)\exp(i\tilde{\mu}_n a) + (\tilde{\mu}_n + \mu_n)\exp(-i\tilde{\mu}_n a)}E_{nz}, \\
C_{nz} &= \frac{2\tilde{\mu}_n}{(\tilde{\mu}_n - \mu_n)\exp(i\tilde{\mu}_n a) + (\tilde{\mu}_n + \mu_n)\exp(-i\tilde{\mu}_n a)}E_{nz}.
\end{aligned} \tag{90}$$

From these we can determine the Calderon operator for the front, using Eq. (16):

$$\mathbf{C}_1(\mathbf{E}_{\mathrm{T}}) = \lim_{y\to 0-}[-\hat{\mathbf{y}}\times(\nabla\times\mathbf{E}_1)]_{\mathrm{T}}(x,y) = i\sum_{n=-\infty}^{\infty}\frac{\exp(i\lambda_n x)}{\tilde{\mu}_n}\begin{bmatrix}\alpha_n n_{\mathrm{r}}^2 k^2 E_{nx}\\ \\ \beta_n\tilde{\mu}_n^2 E_{nz}\end{bmatrix}, \tag{91}$$

where α_n and β_n are as given in Eqs. (30).

The admittance map for the back of the structure, $\mathbf{C}_2$, is given by an identical expression, with n_{r} and a there corresponding to the relative refractive index and thickness of the rear glass substrate, and with the $\mathbf{E}_n$ coming from transforms of the total field along the rear interface:

$$\mathbf{E}_{n\mathrm{T}} = \frac{1}{2L}\int_{-L}^{L}\exp(-i\lambda_n x)\mathbf{E}_{\mathrm{T}}(x,d)\,\mathrm{d}x. \tag{92}$$

In fact, by virtue of the symmetries of our problem, the analogous outer solution field $\mathbf{E}_2(x,y)$ associated with the operator $\mathbf{C}_2$ (defined on $d<y<\infty$) can be expressed

in terms of $\mathbf{E}_1(x,y)$ via

$$\mathbf{E}_2(x,y) = \begin{bmatrix} E_{1x}(x,d-y) \\ -E_{1y}(x,d-y) \\ E_{1z}(x,d-y) \end{bmatrix} \tag{93}$$

and satisfies

$$[\hat{\mathbf{y}} \times (\nabla \times \mathbf{E}_2)]_{\mathrm{T}}(x,d+) = [-\hat{\mathbf{y}} \times (\nabla \times \mathbf{E}_1)]_{\mathrm{T}}(x,0-). \tag{94}$$

In a similar way, the external field $\mathbf{E}_3$ associated with the equivalent surface current $\mathbf{g}_1$ satisfies the same vector partial differential equations as $\mathbf{E}_1$, Eqs. (82), as well as the same quasi-periodicity and interface conditions. The problem formulations for the fields differ only in the boundary condition,

$$\mathbf{E}_{3\mathrm{T}}(x,0) = \mathbf{0}, \quad -L < x < L, \tag{95}$$

and radiation condition: $\mathbf{E}_3 - \mathbf{E}_{\mathrm{inc}}$ is outward propagating as $y \to -\infty$. The solution can be represented in the form

$$\mathbf{E}_3(x,y) = \exp(ik_x x) \begin{cases} \exp(i\tilde{k}_y y)\mathbf{A} + \exp(-i\tilde{k}_y y)\mathbf{B}, & -a < y < 0 \\ \exp(ik_y y)\mathbf{E}_0^{\mathrm{inc}} + \exp(-iky(y+a))\mathbf{C}, & -\infty < y < -a, \end{cases} \tag{96}$$

where $\tilde{k}_y = (n_{\mathrm{r}}^2 k^2 - k_x^2)^{1/2} = \tilde{\mu}_0$, from Eq. (85).

The amplitudes $\mathbf{A}$, $\mathbf{B}$, and $\mathbf{C}$ are determined exactly as for $\mathbf{E}_1$ above, from Gauss's law and the interface conditions, and are given by

$$\begin{aligned} A_x &= \frac{2\tilde{k}_y \exp(-ik_y a) E_{0x}^{\mathrm{inc}}}{(n_{\mathrm{r}}^2 k_y - \tilde{k}_y)\exp(i\tilde{k}_y a) + (n_{\mathrm{r}}^2 k_y + \tilde{k}_y)\exp(-i\tilde{k}_y a)}, \\ B_x &= \frac{-2\tilde{k}_y \exp(-ik_y a) E_{0x}^{\mathrm{inc}}}{(n_{\mathrm{r}}^2 k_y - \tilde{k}_y)\exp(i\tilde{k}_y a) + (n_{\mathrm{r}}^2 k_y + \tilde{k}_y)\exp(-i\tilde{k}_y a)}, \\ C_x &= -\frac{(n_{\mathrm{r}}^2 k_y + \tilde{k}_y)\exp(i\tilde{k}_y a) + (n_{\mathrm{r}}^2 k_y - \tilde{k}_y)\exp(-i\tilde{k}_y a)}{(n_{\mathrm{r}}^2 k_y - \tilde{k}_y)\exp(i\tilde{k}_y a) + (n_{\mathrm{r}}^2 k_y + \tilde{k}_y)\exp(-i\tilde{k}_y a)} \exp(-ik_y a) E_{0x}^{\mathrm{inc}}, \end{aligned} \tag{97}$$

and

$$
\begin{aligned}
A_z &= \frac{2k_y \exp(-ik_y a) E_{0z}^{\text{inc}}}{(\tilde{k}_y - k_y)\exp(i\tilde{k}_y a) + (\tilde{k}_y + k_y)\exp(-i\tilde{k}_y a)}, \\
B_z &= \frac{-2k_y \exp(-ik_y a) E_{0z}^{\text{inc}}}{(\tilde{k}_y - k_y)\exp(i\tilde{k}_y a) + (\tilde{k}_y + k_y)\exp(-i\tilde{k}_y a)}, \\
C_z &= -\frac{(\tilde{k}_y + k_y)\exp(i\tilde{k}_y a) + (\tilde{k}_y - k_y)\exp(-i\tilde{k}_y a)}{(\tilde{k}_y - k_y)\exp(i\tilde{k}_y a) + (\tilde{k}_y + k_y)\exp(-i\tilde{k}_y a)} \exp(-ik_y a) E_{0z}^{\text{inc}},
\end{aligned}
\tag{98}
$$

with

$$
A_y = -\frac{k_x}{\tilde{k}_y} A_x, \quad B_y = \frac{k_x}{\tilde{k}_y} B_x, \quad C_y = \frac{k_x}{\tilde{k}_y} C_x. \tag{99}
$$

From these we can determine the equivalent surface current on Γ_1, using Eq. (21):

$$
\begin{aligned}
\mathbf{g}_{1\mathrm{T}}(x) &= \lim_{y \to 0-} [\hat{\mathbf{y}} \times (\nabla \times \mathbf{E}_3)]_{\mathrm{T}}(x, y) \\
&= -4i \exp(ik_x x) \begin{bmatrix} \dfrac{n_{\mathrm{r}}^2 k^2 \exp(-ik_y a) E_{0x}^{\text{inc}}}{(n_{\mathrm{r}}^2 k_y - \tilde{k}_y)\exp(i\tilde{k}_y a) + (n_{\mathrm{r}}^2 k_y + \tilde{k}_y)\exp(-i\tilde{k}_y a)} \\ \dfrac{k_y \tilde{k}_y \exp(-ik_y a) E_{0z}^{\text{inc}}}{(\tilde{k}_y - k_y)\exp(i\tilde{k}_y a) + (\tilde{k}_y + k_y)\exp(-i\tilde{k}_y a)} \end{bmatrix},
\end{aligned}
\tag{100}
$$

as given in Eq. (39).

References

1. Em. E. Kriezis and S. J. Elston, "A wide angle beam propagation method for the analysis of tilted nematic liquid crystal structures," J. Mod. Opt. **46**, 1201–1212 (1999).

2. Em. E. Kriezis and S. J. Elston, "Light wave propagation in periodic tilted liquid crystal structures: a periodic beam propagation method," Liquid Crystals **26**, 1663–1669 (1999).

3. Em. E. Kriezis and S. J. Elston, "A wide angle beam propagation method for liquid crystal device calculations," Appl. Opt. **39**, 5707–5714 (2000).

4. A. A. Fuki, Yu. A. Kravtsov, and O. N. Naida, *Geometrical Optics of Weakly Anisotropic Media* (Gordon and Breach, Amsterdam, 1998).

5. J. A. Reyes, "Ray propagation in nematic droplets," Phys. Rev. E **57**, 6700–6705 (1998).

6. J. A. Reyes, "Ray propagation in anisotropic inhomogeneous media," J. Phys. A **32**, 3409–3418 (1999).

7. G. Panasyuk, J. Kelly, D. W. Allender, and E. C. Gartland, "Geometric optics approach in liquid crystal films with three dimensional director variations," to appear in Phys. Rev. E.

8. B. Witzigmann, P. Regli, and W. Fichtner, "Rigorous electromagnetic simulation of liquid crystal displays," J. Opt. Soc. Am. A **15**, 753–757 (1998).

9. Em. E. Kriezis and S. J. Elston, "Finite-difference time domain method for light wave propagation within liquid crystal devices," Opt. Commun. **165**, 99–105 (1999).

10. Em. E. Kriezis and S. J. Elston, "Light wave propagation in liquid crystal displays by the 2-D finite-difference time-domain method," Opt. Commun. **177**, 69–77 (2000).

11. Em. E. Kriezis and S. J. Elston, "Numerical modelling of multi-dimensional liquid crystal optics: finite-difference time-domain method," Mol. Cryst. Liq. Cryst. **359**, 289–299 (2001).

12. C. M. Titus, P. J. Bos, J. R. Kelly, and E. C. Gartland, "Comparison of analytical calculations to finite-difference time-domain simulations of one-dimensional spatially varying anisotropic liquid crystal structures," Jpn. J. Appl. Phys. **38**, 1488–1494 (1999).

13. C. M. Titus, J. R. Kelly, E. C. Gartland, S. V. Shiyanovskii, J. A. Anderson, and P. J. Bos, "Asymmetric transmissive behavior of liquid-crystal diffraction gratings," Opt. Lett. **26**, 1188–1190 (2001).

14. G. Bao and D. C. Dobson, "Variational methods for diffractive optics modeling," in *Mathematical Modeling in Optical Science*, G. Bao, L. Cowsar, and W. Masters, eds. (SIAM, Philadelphia, 2001).

15. M. Born and E. Wolf, *Principles of Optics, Sixth Edition* (Pergamon, Oxford, 1991).

16. J. D. Jackson, *Classical Electrodynamics, Second Edition* (John Wiley & Sons, New York, 1975).

17. A. F. Peterson, S. L. Ray, and R. Mittra, *Computational Methods for Electromagnetics* (Institute of Electrical and Electronics Engineers, New York, 1998).

18. M. Cessenat, *Mathematical Methods in Electromagnetism* (World Scientific, Singapore, 1996).

19. J.-C. Nédélec, *Acoustic and Electromagnetic Equations: Integral Representations for Harmonic Problems* (Springer, Berlin, 2001).

20. W. D. Murphy, V. Rokhlin, and M. S. Vassiliou, "Solving electromagnetic scattering problems at resonance frequencies," J. Appl. Phys. **67**, 6061–6065 (1990).

21. X. Chen and A. Friedman, "Maxwell's equations in a periodic structure," Trans. Amer. Math. Soc. **323**, 465–507 (1991).

22. J.-C. Nédélec and F. Starling, "Integral-equation methods in a quasi-periodic diffraction problem for the time-harmonic Maxwell equations," SIAM J. Math. Anal. **22**, 1679–1701 (1991).

23. H. Ammari, N. Bereux, and J.-C. Nédélec, "Resonances for Maxwell's equations in a periodic structure," C. R. Acad. Sci. Paris Sér. I Math. **325**, 211–215 (1997).

24. D. Givoli, *Numerical Methods for Problems in Infinite Domains* (Elsevier, Amsterdam, 1992).

25. A. Taflove, *Computational Electrodynamics, The Finite-Difference Time-Domain Method* (Artech House, Boston, 1995).

26. R. Hiptmair, "Finite elements in computational electromagnetism," Acta Numer. **11**, 237–339 (2002).

27. K.W. Morton and D.F. Mayers, *Numerical Solution of Partial Differential Equations* (Cambridge University Press, Cambridge, 1994).

28. K.S. Yee, "Numerical solution of initial boundary value problems involving Maxwell's equations in isotropic media," IEEE Trans. Antennas Propag. **14**, 302–307 (1966).

29. R. Barrett *et al.*, *Templates for the Solution of Linear Systems: Building Blocks for Iterative Methods* (SIAM, Philadelphia, 1994).

30. C.T. Kelly, *Iterative Methods for Linear and Nonlinear Equations* (SIAM, Philadelphia, 1995).

31. Y. Saad, *Iterative Methods for Sparse Linear Systems* (PWS, Boston, 1996).

32. P. Monk, "A finite element method for approximating the time-harmonic Maxwell equations," Numer. Math. **63**, 243–261 (1992).

33. P. Monk, "An analysis of Nédélec's method for the spatial discretization of Maxwell's equations," J. Comput. Appl. Math. **47**, 101–121 (1993).

34. K.H. Kim, S.B. Park, J.-U. Shim, J. Chen, and J.H. Souk, in *Proceedings of the 4th International Display Workshops* (Nagoya, Japan, 1997), p. 175.

35. S.H. Lee, H.Y. Kim, T.K. Jung, I.C. Park, Y.H. Lee, B.G. Rho, J.S. Park, and H.S. Park, in *Proceedings of the 4th International Display Workshops* (Nagoya, Japan, 1997), p. 97.

36. R. Kiefer, B. Weber, F. Windscheid, and G. Baur, "In plane switching of nematic liquid crystals," in *Proceedings of Japan Display '92*, 547–550 (1992).

37. W. Liu and J. Kelly, "Optical properties of a switchable diffraction grating," Mol. Cryst. Liq. Cryst. **358**, 199–208 (2001).

38. W. Liu, J. Kelly, and J. Chen, "Electro-optical performance of a self-compensating vertically-aligned liquid crystal display mode," Jpn. J. Appl. Phys. **38**, 2779–2784 (1999).

39. N.D. Amarasinghe, "2-D Liquid Crystal Optics via Numerical Solution of Time-Harmonic Maxwell Equations," M.S. thesis, Department of Mathematical Sciences, Kent State University, 2001.

List of Figures

Fig. 3. Finite-element mesh. Horizontal edges correspond to E_x values, vertical edges to E_y, and nodal values to E_z. The nodal and edge values along the right boundary (boxes) indicate degrees of freedom removed by the quasi-periodicity conditions (45).

Fig. 4. Director field of one periodic cell (8×5 μm) of idealized In Plane Switching (IPS) device in the on state.

Fig. 5. Calculated intensities (relative to incident) of reflected and transmitted radiation at the front ($y = 0$) and back ($y = 5$ μm) interfaces for IPS-mode cell of Fig. 4: no polarizers (top), crossed polarizers (bottom).

Fig. 6. Calculations of Liu and Kelly[37] using Beam Propagation Method (BPM) and Geometric Optics Approximation (GOA) of intensity of transmitted radiation at the back ($y = 5$ μm) interface for IPS-mode cell of Fig. 4: no polarizers (top), crossed polarizers (bottom).

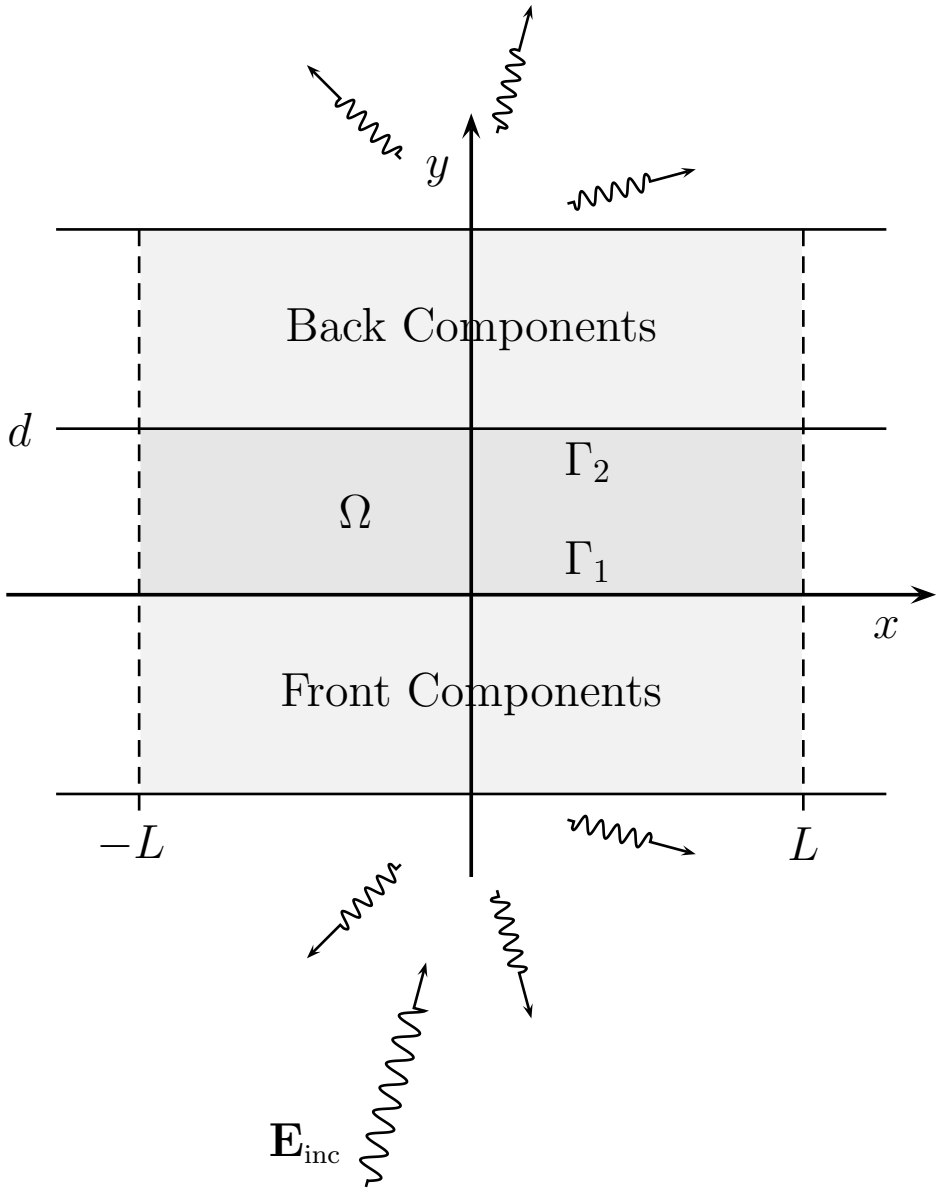

Figure 1, Amarasinghe et al.

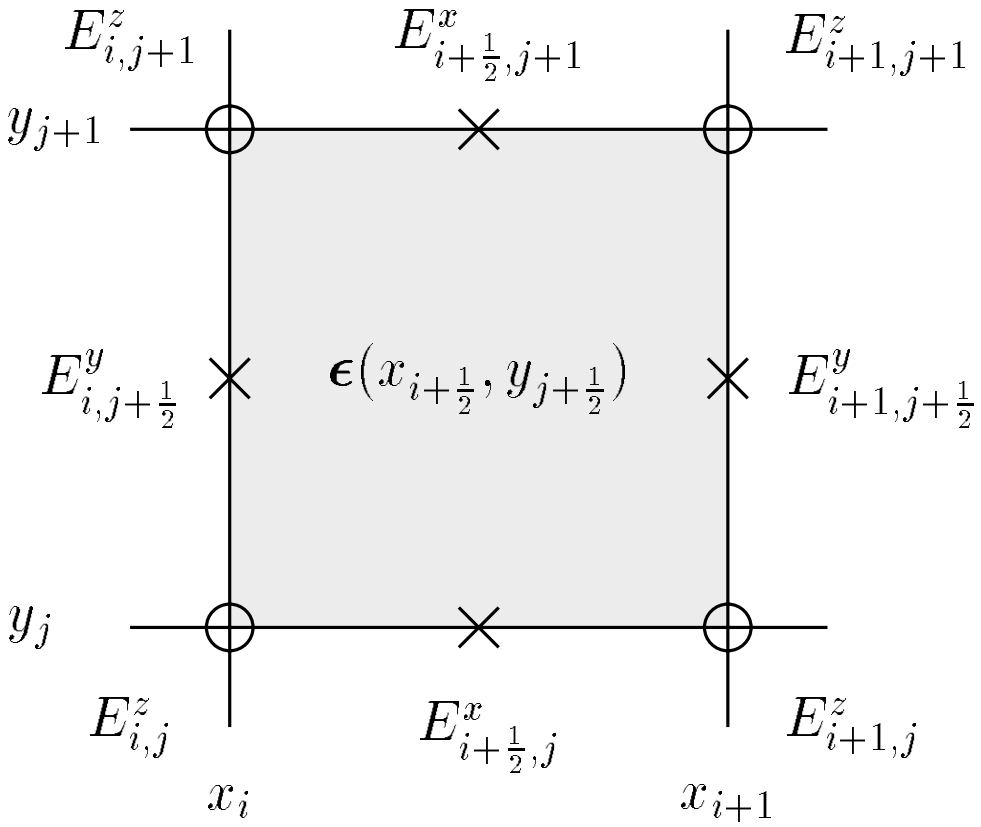

Figure 2, Amarasinghe et al.

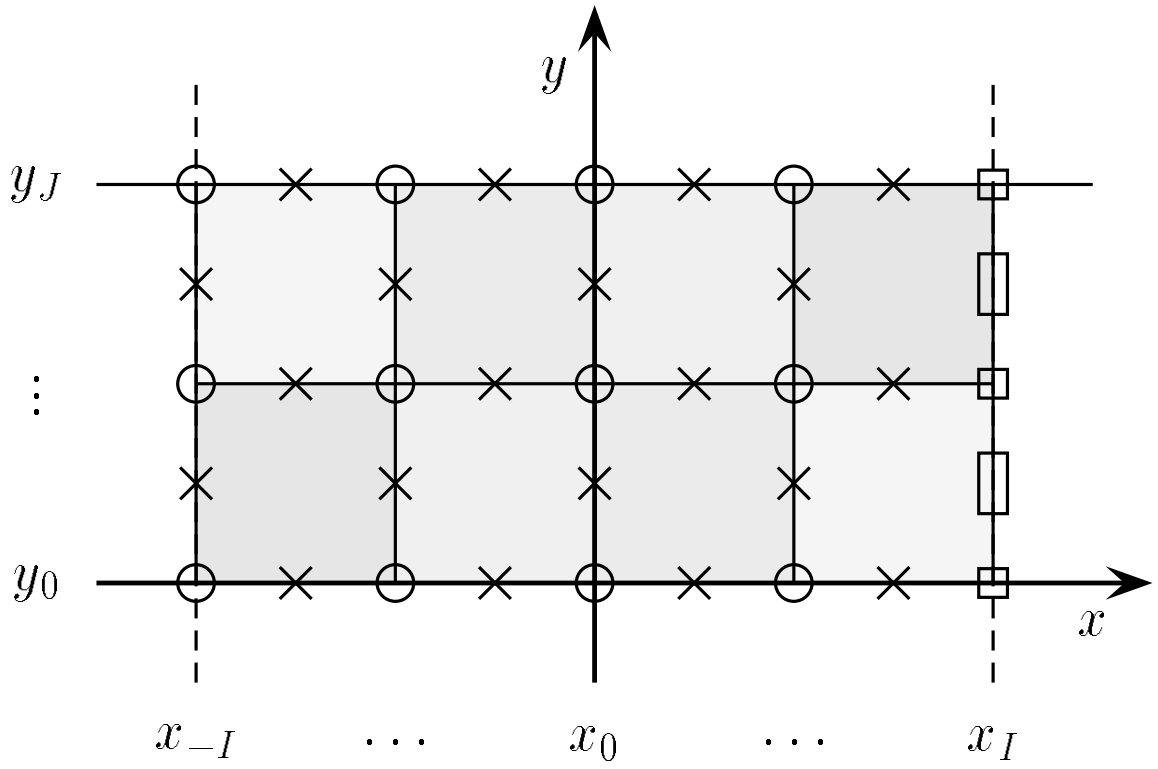

Figure 3, Amarasinghe et al.

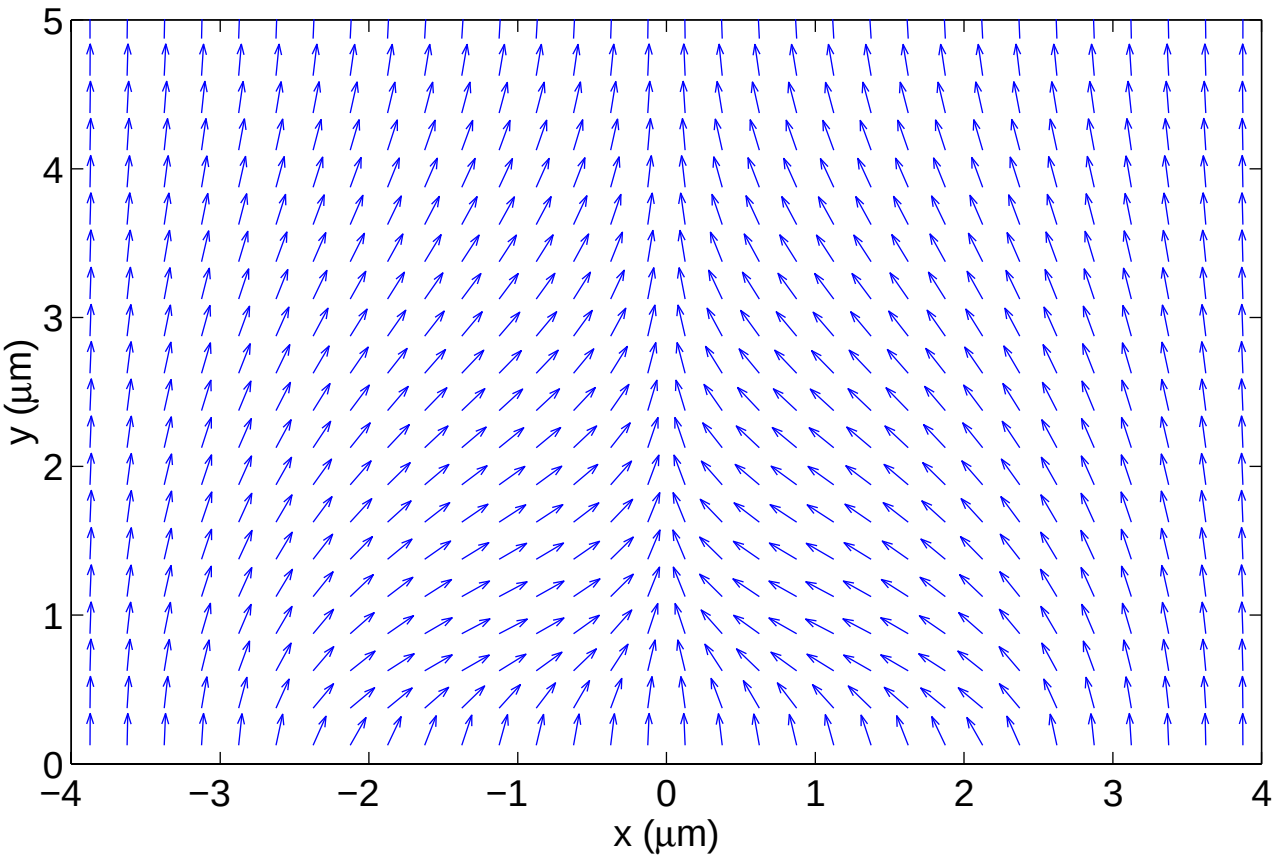

Figure 4, Amarasinghe et al.

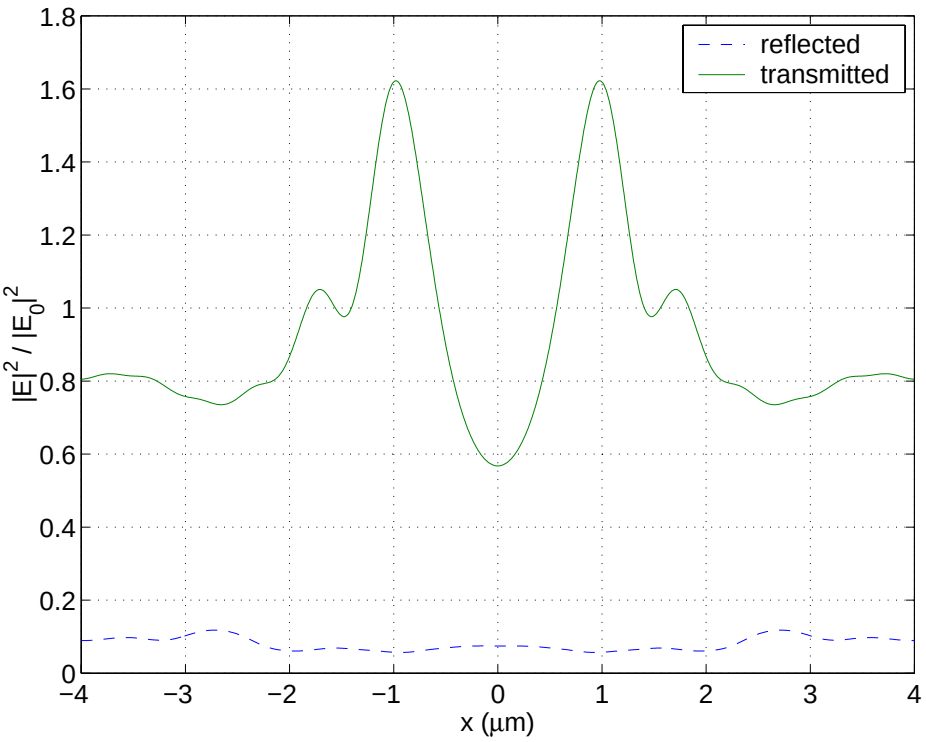

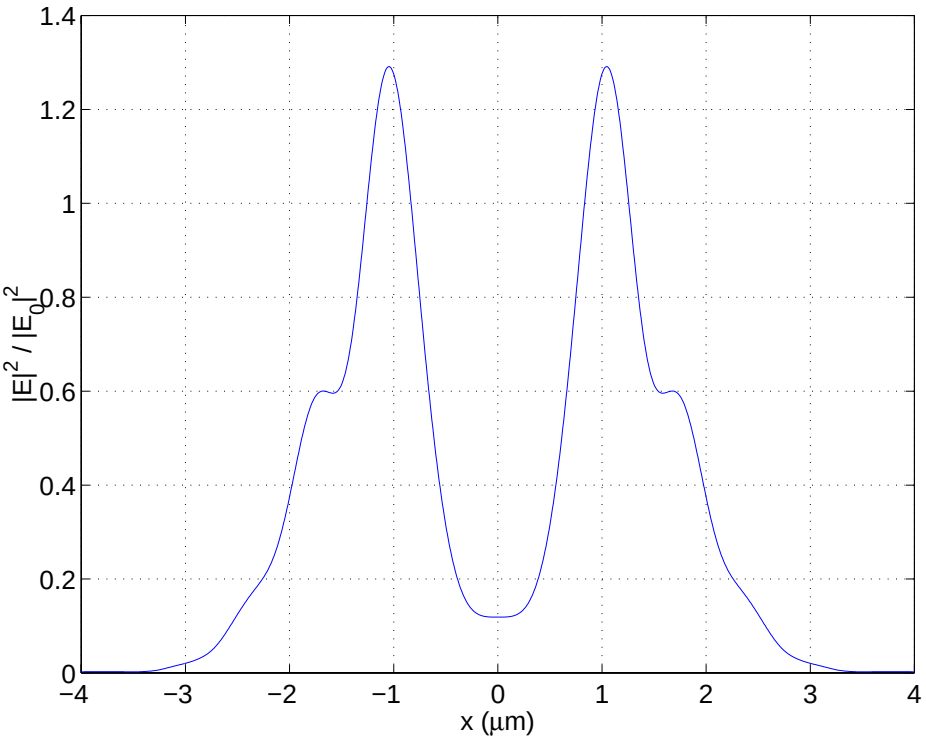

Figures 5ab, Amarasinghe et al.

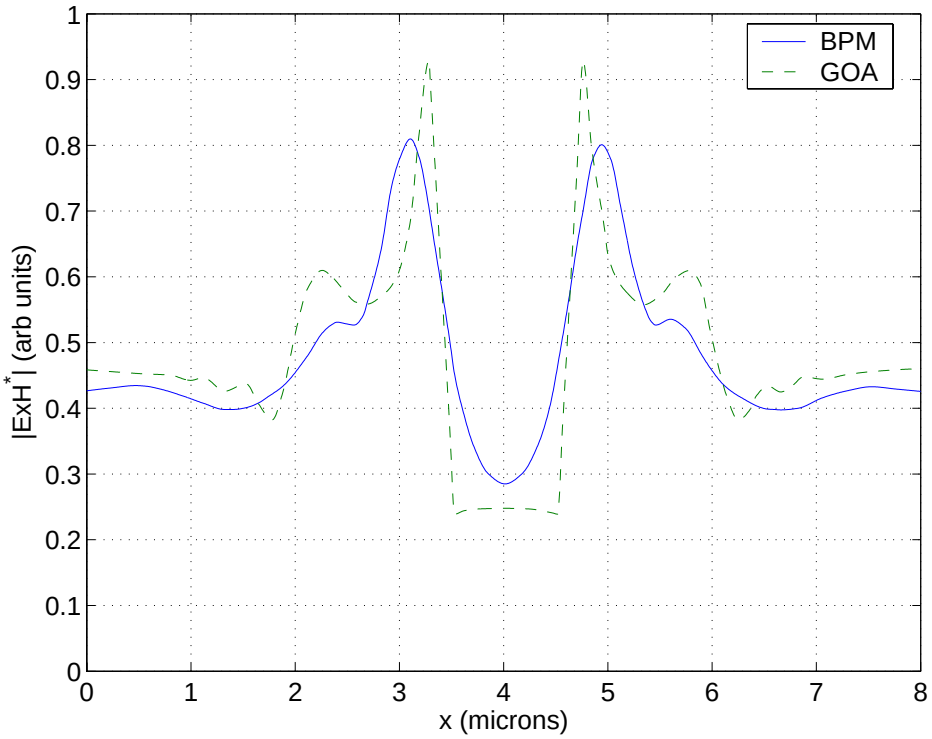

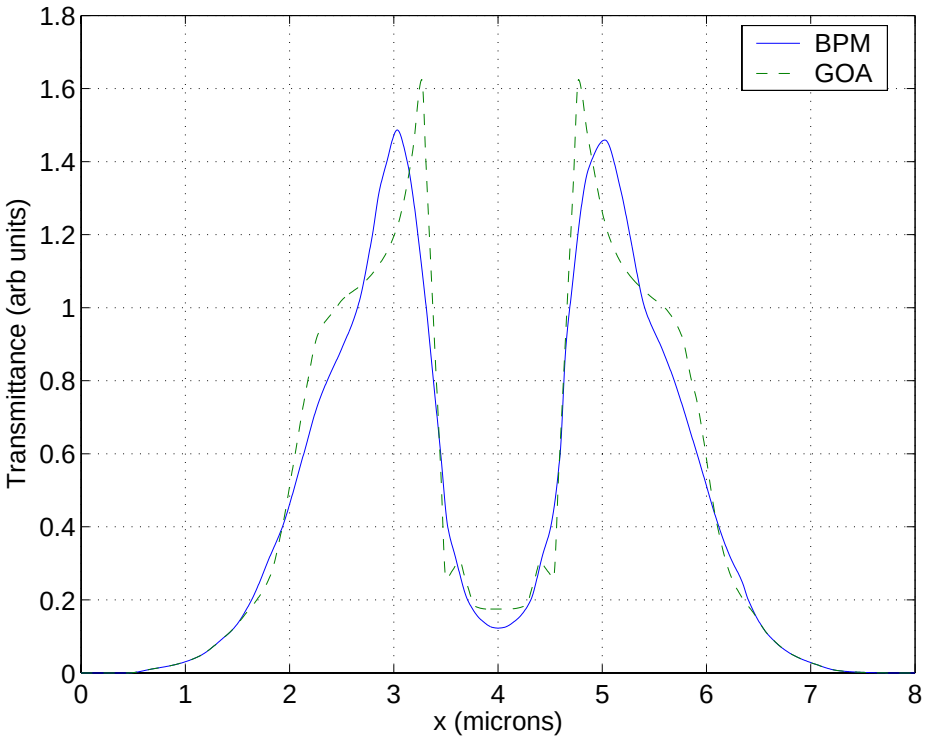

Figure 6ab, Amarasinghe et al.

Table 1. Maximum pointwise errors in discrete approximate solution for test problem with a homogeneous, isotropic film layer of index of refraction $n_{\mathrm{r}} = 1.5$ surrounded by a free space. Problem parameters: incident light $\mathbf{E}_{\mathrm{inc}}(x, y) = \exp(i2\pi y)\hat{\mathbf{z}}$ (normal incidence, z polarized, free-space wavelength = 1 unit), film thickness $d =$ film half-period $L = \frac{2}{3}$ (= 1 wavelength of light in the film). Discretization parameters: half-number of x grid cells $I =$ number of y grid cells J.

I, J	Max error
8	0.145
16	0.356×10^{-1}
32	0.100×10^{-1}
64	0.262×10^{-2}
128	0.669×10^{-3}

Table 1, Amarasinghe et al.

Table 2. Time (in seconds on a 240-MHz PA-RISC workstation) and number of iterations to solve test problem (homogeneous, isotropic film layer of index of refraction $n_{\mathrm{r}} = 1.5$ surrounded by a free space) using Bi-CGSTAB iterative algorithm with and without preconditioning. Problem parameters: incident light $\mathbf{E}_{\mathrm{inc}}(x, y) = \exp(i2\pi y)\hat{\mathbf{z}}$ (normal incidence, z polarized, free-space wavelength = 1 unit), film thickness d = film half-period $L = \frac{2}{3}$ (= 1 wavelength of light in the film). Discretization parameters: half-number of x grid cells I = number of y grid cells J, zero-vector initial guess, 10^{-4} maximum absolute error stopping tolerance.

	Not preconditioned		Preconditioned	
I, J	Iterations	Time (s)	Iterations	Time (s)
8	451	1.70×10^1	4	0.00
16	1,702	2.68×10^2	4	1.00
32	6,190	3.93×10^3	4	4.00
64	23,654	4.91×10^4	4	1.80×10^1
128			4	8.70×10^1

Table 2, Amarasinghe et al.